International Journal of Environment and Geoinformatics 10(3):154-175 (2023)

Research Article

A Numerical Study of the Flow Patterns around Midchannel Islands in Lowland Rivers and Their Possible Biogeomorphological Impacts

Naghmeh Heidari[1,*], Murat Aksel[2,3], Oral Yagci[2,4], Manousos Valyrakis[5]

[1] Civil Engineering Department, Faculty of Hydraulics and Water Resources, Istanbul Technical University, Istanbul, TURKIYE
[2] HECLAB Research and Technology Center, ITU, Istanbul Technical University, TURKIYE
[3] Civil Engineering Department, Alanya Alaaddin Keykubat University, Antalya, TURKIYE
[4] Civil Engineering Department, Aydin Adnan Menderes University, Aydin, TURKIYE
[5] School of Engineering, University of Glasgow, Glasgow, UNITED KINGTOM

* Corresponding author: N. Heidari
E-mail: heidari17@itu.edu.tr

Received 29.06.2023
Accepted 30.09.2023

How to cite: Heidari et al., (2023). A Numerical Study of the Flow Patterns around Midchannel Islands in Lowland Rivers and Their Possible Biogeomorphological Impacts, *International Journal of Environment and Geoinformatics (IJEGEO)*, 10(3): 154-175. doi. 10.30897/ijegeo.1320654

Abstract

Midchannel islands (MCIs) are instream geomorphic units generally emerge in lowland rivers. Despite their significant ecomorphological services in the river ecosystem, the flow patterns around these self-forming riparian landforms and their impacts on aquatic life are not fully understood yet. Understanding the flow pattern around these formations enables practitioners to produce cost-effective, sustainable, and eco-friendly river management projects and strategies, forming the motivation of this study. Herein, the secondary flow pattern around MCIs was analyzed by employing a RANS-based numerical model. Flow around the simplified bodies was simulated to give a more precise analysis regarding flow-island interactions. Once the numerical validation process was completed for the cylinder using an experimental dataset, the validated model was implemented for islands (streamlined island, vertically sloped island (VSI), and realistically sloped island (RSI)). Analysis of the model results revealed the following key findings: 1) the RSI acted like a streamlined object and produced weaker lee-wake vortices with a longer recovery distance compared to the streamlined island and the VSI, 2) the RSI gained a better-streamlined form near the bed than near the water surface due to enhanced elongation, 3) this situation in the RSI case generated highly variable flow patterns along the depth behind the MCI, and 4) due to the three-dimensional geometry of the RSI, the generated large-scale vortices propagated asymmetrically towards the sides of the channel rather than remaining around the centerline.

Keywords: computational fluid dynamics, midchannel island, lowland rivers, wake hydrodynamics, secondary flow

Introduction

Midchannel islands (MCI) are bar formations stabilized by vegetation colonization that emerge in active river corridors. These geomorphic units usually arise near the lowland zones of basins due to a decrease in sediment size, channel bottom slope, and bed shear stresses in the streamwise direction. Under the cycle of discharge and sediment flux fluctuations, these self-forming units may be capable of altering riverine morphology and ecology on long-time scales (Heidari et al., 2021) with their ecological services. Midchannel islands significantly impact flow variability and channel geomorphology in river corridors. Biodiversity and ecological integrity can be enhanced more rapidly by flow variability in natural rivers (Lloyd et al., 2003; Poff and Zimmerman, 2010). Nutrient dynamics increases by vertical exchange of surface–subsurface water (Maazouzi et al., 2012) in the wake region of midchannel islands. Moreover, the wetted area of the hyporheic zone increases due to rising water depths and reduced velocity and turbulence in the upstream area of the island, which leads to improved aquatic life and water quality (Heidari, 2021).
Enhancing the flow efficiency and maintaining the secondary channels by midchannel islands lead to significant effect on the river reach in longer distances (Leli and Stevaux, 2021). A better understanding of the hydrodynamics around a midchannel island, which plays a crucial role in bilateral interaction between flow-vegetation-sediment, helps practitioners to produce cost-effective, sustainable river management projects. More specifically, investigating the flow patterns around an island helps to realize their impacts on sedimentation and morphological processes.

The island's presence generally increases hydraulic resistance in the active channel (Gurnell and Petts, 2002; Wilson et al., 2006). The formation of midchannel islands can be either deposition-based or erosion-based. In deposition-based cases, they emerge downstream of in-stream vegetation or colonizing saplings with enough cohesion with river bed depositions. In the latter case, the island can be excised from a continuous floodplain (Nanson and Knighton, 1996; Tooth and Nanson, 1999). Instream processes, which are driven by reciprocal dynamic relationships between river components, and offstream processes have been studied by several reserachers (e.g., Latrubesse and Stevaux, 2015; Leli, 2018; Leli et al., 2020). Edwards et al. (1999) pointed out that the incipience of midchannel islands remarkably

depends on large woody debris, providing an excellent condition for rapid plant colonization and entrapment of organic and inorganic matter. The island erosion in high flows can lay the groundwork for the initiation of other pioneer islands in the river corridor, and uprooted plants by major floods can regrow on new bars (Edwards et al., 1999; Kollmann et al., 1999). The development of pioneer islands is associated with flow regimes and sedimentation rates (Gurnell and Petts, 2002). The sedimentation rate is highly influenced by vegetation density, plant size, and the number of stems (Thornton et al., 1997; Francis et al., 2006). However, according to Francis et al. (2006), there is a lack of consistent patterns for the impact of vegetation type and species on sediment caliber.

The field experience documented by Callow and Smettem (2007) is a good example of demonstrating vegetation's formative role in river eco-morphology. With their long-term reflections on river morphology, these plants can be regarded as ecological engineers (Schoelynck et al., 2012). In the laterally unconfined river reaches with non-cohesive material (Murray and Paola, 1994; Brierley and Fryirs, 2005), flow can freely modify the spatial planform pattern of the channel. In such reaches, the excess scour in flow convergence leads to transportation of the load and its deposition in the downstream area of flow divergence, which induces the initiation of midchannel bars (Murray and Paola, 1994; Ashworth et al., 2000). Subsequently, the flow variables govern the emergence of riparian vegetation (Poff et al.,1997), and vegetation assists the bar stabilization (Leopold and Wolman, 1957; Eekhout et al., 2013; Li et al., 2014) by depositional processes (Yagci et al., 2016; and Yagci et al., 2017). The asymmetric geometry of the midchannel island leads to deflection of the flow to one side of the downstream zone (Nicholas and Sambrook-Smith, 1999), which changes the channel planform. Moreover, the flood sequences change the braided channel's morphology because midchannel islands bring about channel narrowing and incision (Knighton, 1972; Surian and Rinaldi, 2004; Luchi et al., 2010).

Evaluating the streamwise velocity enables estimating the sediment transport capacity, which helps to predict the channel morphodynamics. The cause of channel adjustments, where midchannel islands exist, is changing sediment fluxes by instream formations and vegetation density. Vegetation reduces the sediment yield and stabilizes the riverbanks consistently, leading to long-term meander development (Carson, 1984; Leigh, 2006). Hook (1986) compared meandering rivers and showed that midchannel bars increase the curve of meander bends by causing sediment redistribution and channel shifting. Meandering rivers' morphodynamics is mainly controlled by erosion processes and secondary flow effects downstream of the curves (Keylock et al., 2012).

Knowledge about the intertwined interaction between flow and sediment around a vegetated patch constitutes important background in understanding pioneer islands' development/expansion process (Gurnell et al., 2012). When a pioneer island triggers the hydraulic disturbance, the island expansion occurs due to the emerging secondary flow (Tooth and Nanson, 1999). Accordingly, as the size of the pioneer island increases, the wake zone becomes larger, and the deposition/erosion processes bring about habitat heterogeneity in the downstream region of the island. The significant role of instream/riparian vegetation in transforming river systems from braided to a single thread is a well-documented fact based on experimental (Tal and Paola, 2007) and field (Gurnell et al., 2012) observations. Therefore, the flow around the emergent vegetation received great attention in recent decades (e.g., Nepf, 1999; Bennett et al., 2008; Euler et al., 2014; Kitsikoudis et al., 2016; Kim et al., 2018; Kitsikoudis et al., 2020).

The recirculation zones forming in natural river corridors are influential factors in trapping nutrients/micro-organisms (Guo et al., 2020; Yagci and Strom, 2022). In line with this vision, some researchers have gone beyond the patch scale analysis and investigated the island dynamics as a solid body exposed to the flow by conducting both experimental and numerical models (e.g., Lloyd and Stansby, 1997a; Lloyd and Stansby, 1997b; Ouro. et al., 2017), in which the island geometry was simplified/reduced to a conical body. However, many questions regarding the flow patterns around the realistic geometry of a midchannel island remained unanswered. When the midchannel formations become stabilized by vegetation (Leopold and Wolman, 1957; Yagci and Strom, 2022), the secondary flows bring about bar elongation (Ashworth, 1996; Wintenberger, 2015) and asymmetrical growth (Ashmore, 1993). Changing the planform of the obstacle from circular to elongated one modifies the flow characteristics and scour mechanism (Chang et al., 2013b; Kitsikoudis et al., 2017). According to Chang et al. (2013b), elongation weakens the horseshoe vortex and triggers more streamlined separated shear layers near the bed.

This study is a continuation of the study by Heidari et al. (2021), which aimed to investigate the influence of MCI on river morphology. Differing from our previous study, i.e., Heidari et al. (2021), in this study, we aim to investigate the impact of an isolated midchannel island on the flow domain and its probable consequences on aquatic life. A Reynolds-Averaged Navier Stokes (RANS) based numerical model was used to attain this objective. In order to analyze the flow pattern around the midchannel island, flow around the simplified obstacles (i.e., 2D bodies) was firstly investigated. These obstacles included emergent circular cylinders, streamlined and vertical-sloped islands (VSI). To increase the reliability of the results, first, the analysis was done for a circular cylinder due to the availability of the experimental dataset. Then the planform of the obstacle was altered to form an island by a transition from a streamlined object, which is a well-known hydrodynamic form in literature. Finally, based on the knowledge obtained from these 2D bodies from the same numerical domain, the influence of realistic-sloped islands (RSI) on flow patterns was discussed in detail. This type of multi-staged approximation allowed us to identify the role of morphometric features of the RSI on the observed flow pattern. The present study explores the

following research questions within an ecohydrological context:

1) First, the influence of the three-dimensional geometry of a midchannel island on the structure of generated lee-wake vortices is investigated, considering the perturbative role of lee-wake vortices in the planform of a river reach (i.e., helical flow structure, meandering process).
2) Second, considering that large-scale secondary flow patterns (e.g., LSCRVs) may generate upwelling or downwelling processes, it is imperative to study the effect of a midchannel island's three-dimensionality on the vertical momentum transfer in its wake region.
3) Third, it is important to explore the impact of a midchannel island's three-dimensional geometry on boundary layer separation processes and bed shear stresses around it, given that flow patterns generated near the bed may control riverbed morphology, vegetation distribution, and fish spawning processes.

Methodology

Flow 3D is a numerical tool allowing the development of an insight into the role of geometrical features of the island-like obstacle on generated flow patterns. The RANS model was calibrated accurately for an emergent circular cylinder initially based on an experimental dataset produced by Kitsikoudis et al. (2016). The experimental and numerical data comparison is given below in the sub-section of "2.2 Model Validation". Later, the initial and boundary conditions of the calibrated model were kept constant, and the emergent circular cylinder was replaced with other obstacles to build knowledge regarding the role of geometrical components (e.g., the role of streamlining, the frontal, and side slopes) and the produced flow patterns. The geometric features of the examined obstacles are given in Figure 1, and the reason behind their selection is summarized in Table 1.

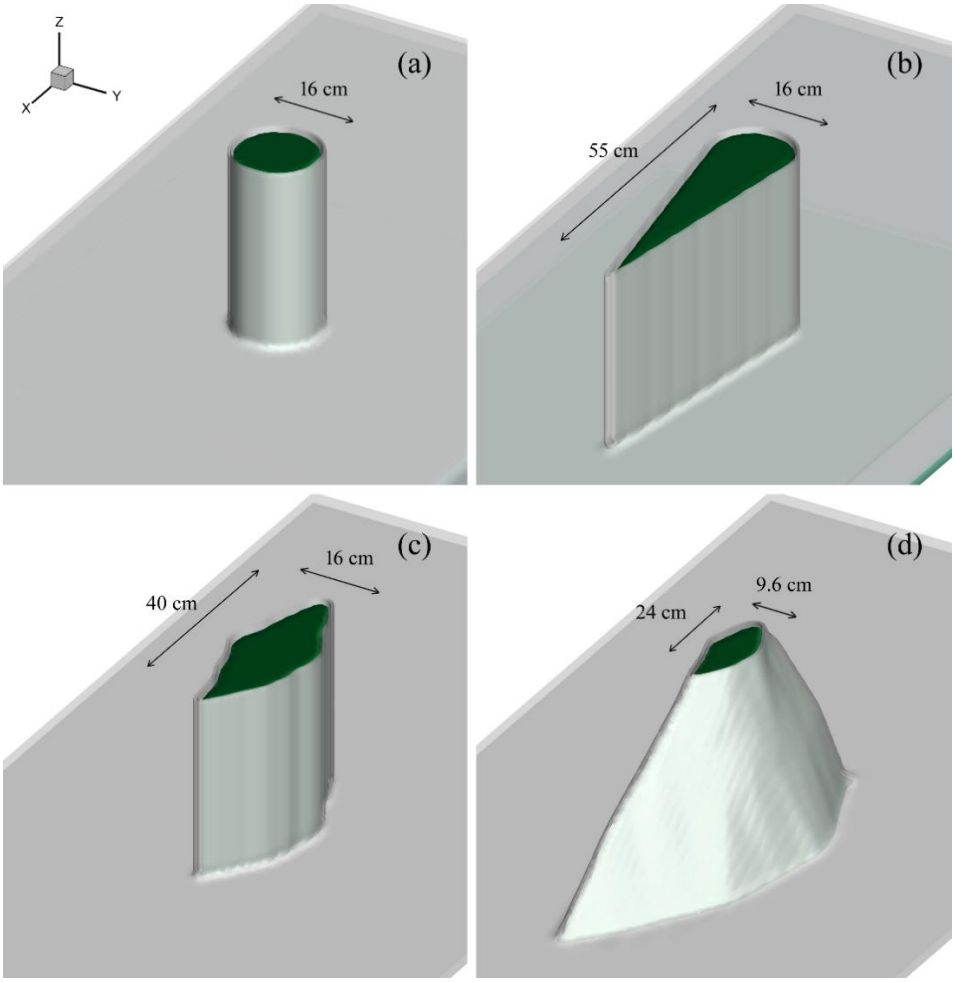

Fig. 1. The geometry of the a) Cylinder, b) Streamlined Island, c) Vertical-Sloped Island (VSI), and d) Realistic-Sloped Island (RSI).

Satellite views belonging to the Maritsa basin were utilized to choose the island-like geometry. A characteristic island from the community of MCIs was chosen as a geomorphological feature representative of island-like geometries (Figure 2). Subsequently, the morphometric ratios belonging to the planform view of this island were used in the models of VSI and RSI.

Table 1. The numerical scenarios examined in the study.

Obstacle	Objective
Cylinder	**Reference case (validated by experimental dataset).** Since the flow around an emergent cylinder is a well-known case in the pertinent literature, this body was taken as the reference case. The calibration of the numerical model was carried out for this reference case based on the experimental dataset produced by Kitsikoudis et al. (2016).
Streamlined Island	**Quasi-reference case:** The flow around this form of obstacle is known in the literature. The projection area against the flow was kept constant. A half-cylinder, which has an identical diameter with the aforementioned reference case, was placed in front of it. The main idea behind this approximation was to make a direct comparison with cylinder, and to observe the consequences of streamlining effect on the flow structure.
Vertical-Sloped Island (VSI)	**The simplified form of target case, i.e., island-like obstacle:** The 2D form of the island with vertical face was exposed to identical flow conditions. In this way, only the role of island planform on the flow domain was investigated, and the influence of slopes was excluded. Such a decomposition enabled us to understand the significance of the "island planform" and "the surrounding slopes" on the observed flow field separately.
Realistic-Sloped Island (RSI)	**The target case, i.e., island-like obstacle:** The flow field around the island-like obstacle was investigated. Differing from the previous case, the sloped surrounding walls were also included in the simulations. It was thought that the differences in numerical outcomes between the previous case and this case were basically due to the sloped walls around the island.

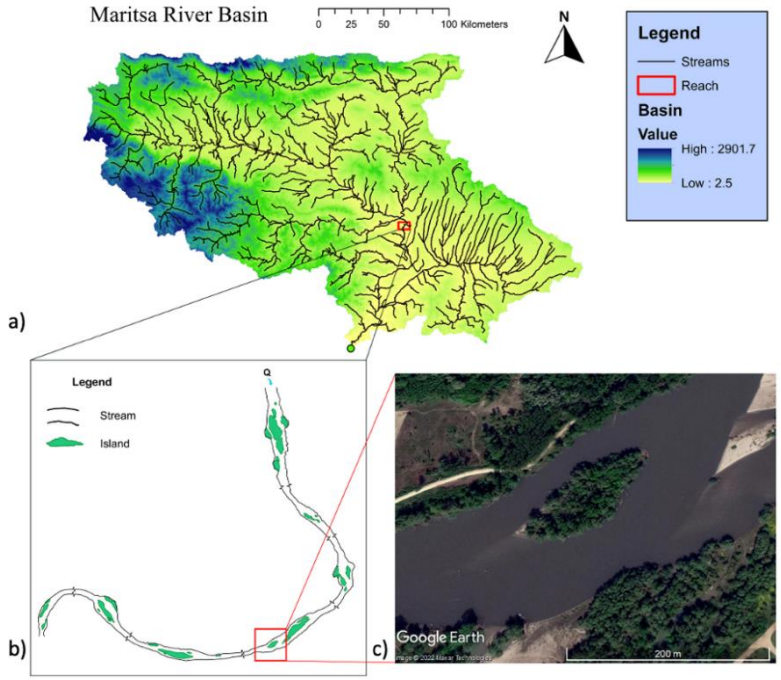

Fig. 2. The plan view of the selected MCI in Maritsa Basin: a) the drainage pattern and distribution of altitude of Maritsa basin, b) river reach which accommodates a family of islands, c) close-up view of the selected MCIs.

The numerical simulations were conducted in a rectangular flume with 6 m length, 1 m width, and 0.35 m depth. These dimensions were chosen to be compatible with the experimental dataset used for the calibration. Initial fluid elevation in the flume inlet was 0.31 m, the same as the experiments. The aforementioned four emergent obstacles (i.e., cylinder, streamlined island, VSI, and RSI) were exposed to identical flow conditions during the numerical simulations. For all scenarios, the projected area was the same, and the RSI case's blockage ratio matched the obstacles with vertical walls. The side and front slopes of the RSI were 1V/2H, and the lee-side slope was 1V/3H; herein, V and H denote vertical and horizontal distances, respectively. A mesh grid was utilized by employing the nested grid approach. The nested grid was applied to the domain where the flow patterns emerged, and the convective acceleration/deceleration was pronounced. The model characteristics and boundary conditions were prepared based on the study by Aksel et al. (2021), which includes all the authors of this paper, and the cylinder case was verified with an experimental study by Kitsikoudis et al. (2016). Further details about the model are given below.

Hydrodynamic model

Numerical simulations were carried out by using flow-3D software based on Reynolds-Averaged Navier-Stokes (RANS) equations, including (1) the law of conversation of mass for an incompressible fluid:

$$\frac{\partial}{\partial x}(uA_x) + \frac{\partial}{\partial y}(vA_y) + \frac{\partial}{\partial z}(wA_z) = 0 \qquad \text{(Eq.1)}$$

and (2) the Navier–Stokes momentum equations for an incompressible fluid:

$$\frac{\partial u}{\partial t} + \frac{1}{V_F}\left\{uA_x\frac{\partial u}{\partial x} + vA_y\frac{\partial u}{\partial y} + wA_z\frac{\partial u}{\partial z}\right\} = -\frac{1}{\rho}\frac{\partial p}{\partial y} + F_x$$

$$\frac{\partial v}{\partial t} + \frac{1}{V_F}\left\{uA_x\frac{\partial v}{\partial x} + vA_y\frac{\partial v}{\partial y} + wA_z\frac{\partial v}{\partial z}\right\} = -\frac{1}{\rho}\frac{\partial p}{\partial y} + F_y$$

$$\frac{\partial w}{\partial t} + \frac{1}{V_F}\left\{uA_x\frac{\partial w}{\partial x} + vA_y\frac{\partial w}{\partial y} + wA_z\frac{\partial w}{\partial z}\right\} = -\frac{1}{\rho}\frac{\partial p}{\partial z} + F_z + G_z \qquad \text{(Eq.2)}$$

where *u*, *v*, and *w* are the fluid velocity components along *x*, *y*, and *z*, respectively, V_F is the fractional volume open to flow, ρ is the fluid density, A_x, A_y, and A_z indicate the fractional area open to flow in x, y, and z directions, respectively, F_x, F_y, and F_z are the viscous accelerations, and G_z is the gravitational acceleration (Flowscience, 2019). Different turbulence models (i.e., k-epsilon, k-ω, Renormalized Group, RNG) were tested during the calibration stage. The comparisons between model outputs and the experimental data revealed that the k-ω turbulence model exhibited significantly higher performance than the other turbulence models. Furthermore, the higher efficiency of the k-ω closure model in simulating boundary layer separation was also previously experienced by Roulund et al., 2005, Baykal et al., 2015, and Larsen et al., 2016. In light of these facts, k-ω turbulence closure was used throughout the modelling study. In defining the boundary conditions, side channels were represented as smooth walls in the model, like the experiments by Kitsikoudis et al. (2016). Furthermore, the upside boundary condition was selected as a pressure-type boundary condition. The relative pressure was defined as zero here. For the inlet boundary condition, the velocity at the channel entrance was set to 0.33 m/s. Reynolds number was 52800, implying that the boundary layer around the cylinder was laminar and the flow was fully turbulent in the wake region (Sumer and Fredsøe, 1997). The water level was set to 0.31 m, which was the case in the experiments by Kitsikoudis et al. (2016). Constant water levels were defined both for the inlet and outlet conditions. The applied mesh number was 1050000 for all the obstacles, and nesting was applied around each obstruction. Mesh sensitivity tests were applied before starting the simulations, and it was seen that the model outputs were independent of the applied mesh number.

Model validation

As stated above, the numerical reference model, which simulates flow around a circular cylinder, was previously calibrated by Aksel et al. (2021). In their model validation, Aksel et al. (2021) compared their numerical outputs with experimental data produced by Kitsikoudis et al. (2016). Later, they extended their numerical analysis for the case of flow around a pile located on the scoured bottom, differing from this study. They compared 13 vertical and 11 horizontal experimental profiles of flow variables (i.e., time-averaged mean flow, turbulence intensities, and turbulence kinetic energies) with numerical model outputs (Figure 4 and 6 in Aksel et al., 2021). The comparisons indicated that the numerical model produces results in harmony with the experimental measurements. For the sake of simplicity, the same comparison was presented here in a different way in Figures 3 and 4 and discussed in the next paragraph.

Generally speaking, for a numerical model simulating the flow around a body, the representation of vortices in the wake region with an acceptable accuracy can be seen as a sign of the model's success to a certain extent. In this context, the plan view of time-averaged streamwise velocity and the lateral turbulence intensity patterns at specific water levels were comparatively presented in Figures 3 and 4, respectively. The main idea behind comparing normalized lateral turbulence intensities in Figure 4 was that this turbulence statistic is a good indicator to compare the pairs of vortices generated in the experimental and numerical flumes. It should also be considered that the separation-induced vortex shedding in the wake region triggers the periodical formation of pronounced oscillation in lateral velocity and thus augments the lateral turbulence intensity. According to Figures 3 and 4, it can be stated that the numerical model yields result in harmony with the experimental data. Further comparison of the numerical data with the experimental measurements can be obtained in Aksel et al. (2021).

As long as the initial/boundary conditions were kept constant, alterations of the geometrical features of the bodies in a numerical model have a limited influence on the model validation. From this motivation, once the numerical model was validated for the obstacle of the emergent circular cylinder, the initial and boundary conditions were kept unchanged. Afterward, the cylinder body was transformed into the examined other three forms, i.e., streamlined island, VSI, and RSI. It might be argued that the absence of a dataset to calibrate all these three cases can be seen as a limitation for the study, which appears to be a legitimate observation upon initial examination. However, it is important to consider that the primary aim of the study was not to quantitatively assess the kinematic variables with a high level of accuracy. Hence it is more appropriate to prioritize the analysis of flow patterns rather than the specific numerical values derived from the model. In this study, the primary objective was to undertake a comparative examination of the flow patterns surrounding the objects, rather of just focusing on the numerical values of the physical variables (such as turbulence kinetic energy or vorticity) produced as outputs from the applied model. Therefore, it was postulated that this evaluation would generate a satisfactory degree of precision for the stated aims of the study.

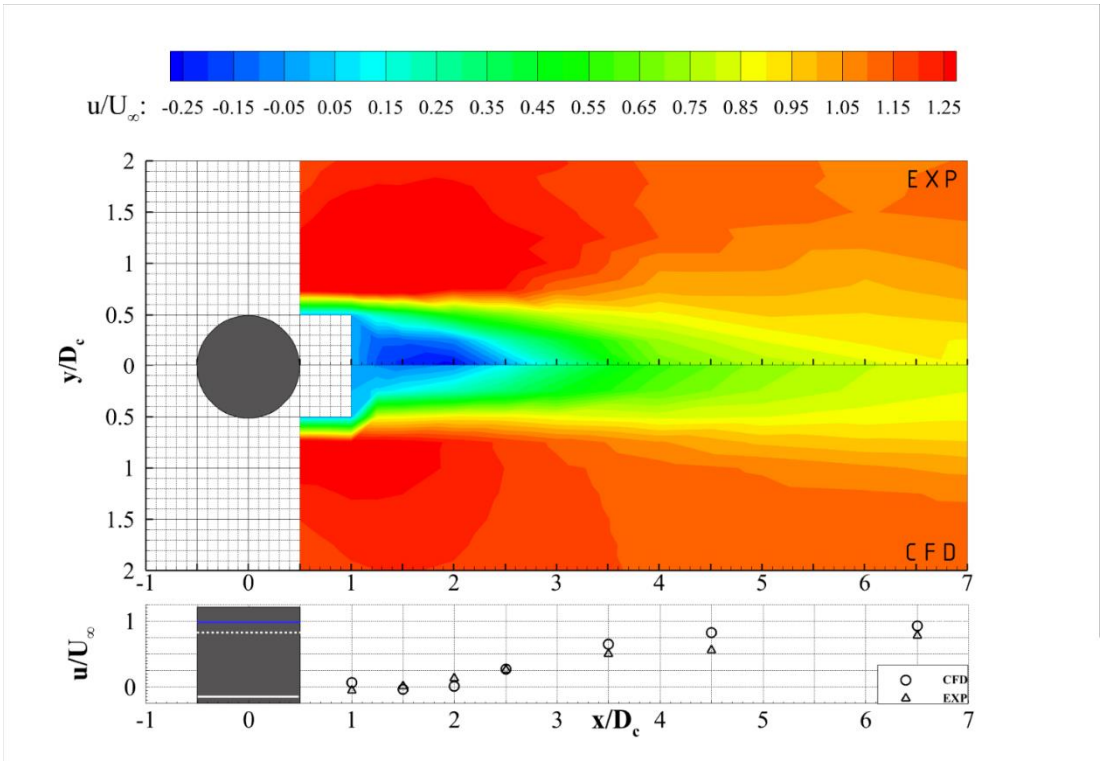

Fig. 3. The comparison of horizontal distributions of time-averaged normalized streamwise velocity, $\bar{u}/U_\infty$, between experimental (Kitsikoudis et al., 2016) and the numerical data for the emergent circular cylinder case. The comparison was fulfilled for the water level of z/H=0.4. The values located on the probe layout given in Kitsikoudis et al. (2016) were employed during this comparison. The lateral profiles which constitute the contour plots can be found in detail in Aksel et al. (2021).

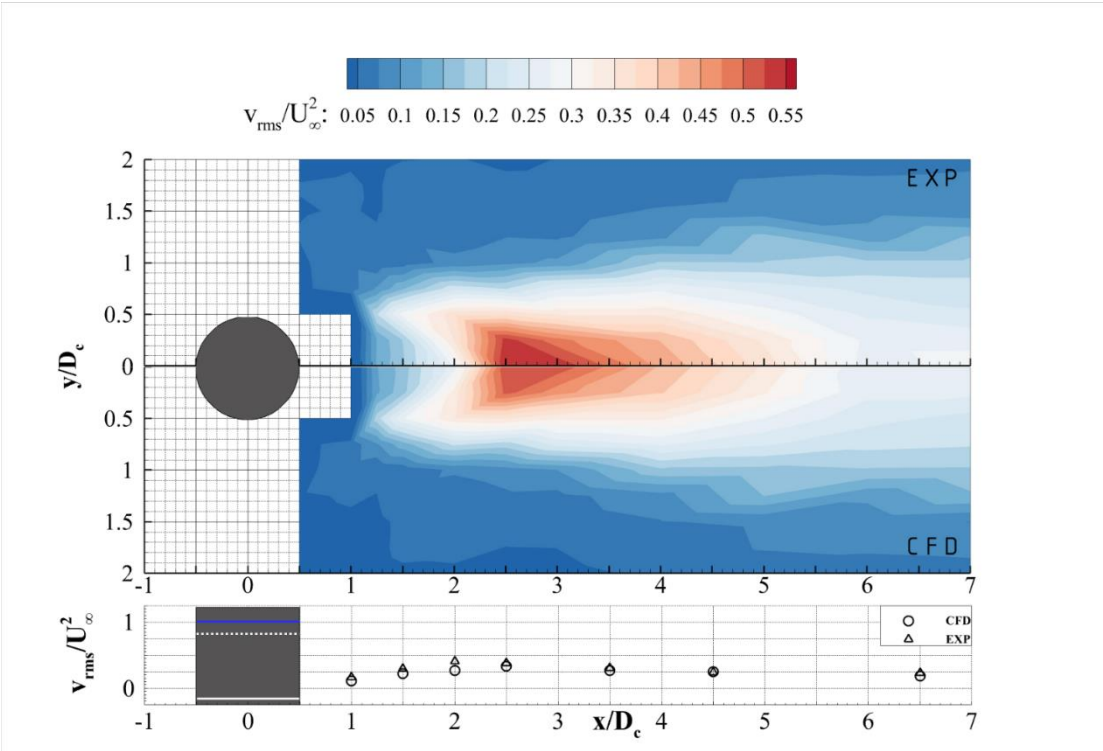

Fig. 4. The comparison of horizontal distributions of time-averaged normalized lateral turbulence intensity, v_{rms}/U_∞^2, between experimental (Kitsikoudis et al., 2016) and the numerical data for the emergent circular cylinder case. The comparison was fulfilled for the water level of z/H=0.4. During this comparison, the values located on the probe layout given in Kitsikoudis et al. (2016) were employed. The lateral profiles which constitute the contour plots can be found in detail in Aksel et al. (2021).

Results

Analysis of streamwise velocity

Time-averaged streamwise velocity patterns offer clues regarding the spatial distribution and strength of energetic events (e.g., lee-wake vortices), which arise from produced flow patterns. The contour plots of the time-averaged normalized streamwise velocity in the vertical plane along the flume centerline and the middle of the contraction region (i.e., the region between the obstacle and channel wall) are presented in Figure 5. It is discernible that the cylinder and VSI acted against the flow similarly in terms of producing severe vortex-induced deceleration zones behind themselves. In the wake region, a severe deceleration zone indicates the occurrence of a strong shear layer behind the body. Hence, the flow recovered quickly for the cylinder and VSI cases because of strong lateral momentum transfer (Figure 5). The deceleration zones that form behind the obstacles were uniformly distributed along the depth for these two cases except near the bed.

On the other hand, the velocity patterns in the recovery region of the streamlined island and RSI were quite similar. Therefore, the gradual recovery observed behind these bodies can be regarded as the natural consequence of relatively weaker vortices that take place behind these obstructions. The similarity between streamlined island and RSI, in a way, confirmed that RSI is a kind of streamlined obstacle. In other words, RSI became more streamlined than VSI along with the depth due to its elongation by the lee-side slope, which is the consequence of the natural self-streamlining mechanism. Therefore, the elongated tail of the RSI leads to its resemblance to the streamlined island case in this study.

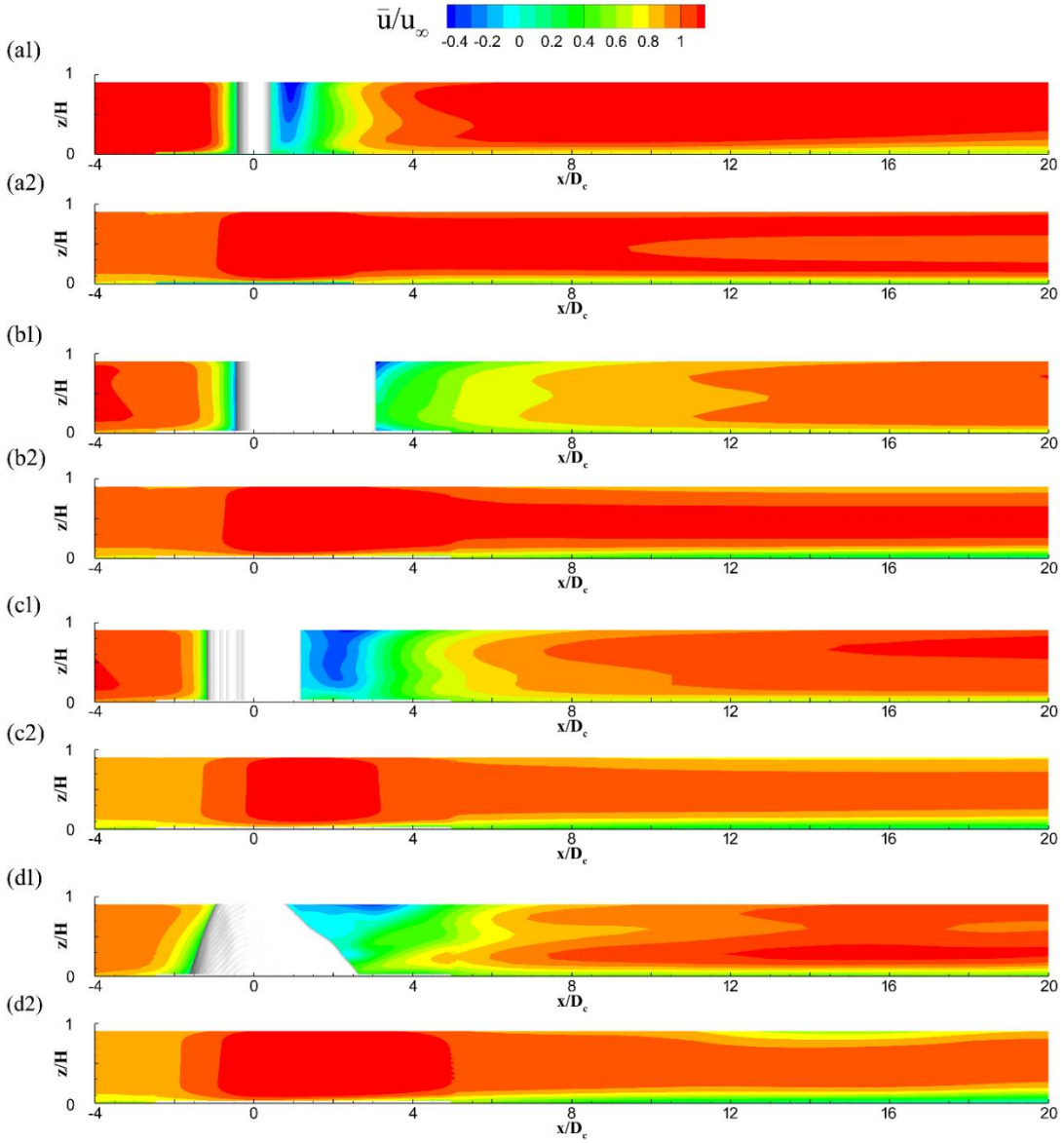

Fig. 5. The contour plots of the time-averaged normalized streamwise velocity, $\bar{u}/U_{\infty}$, in the vertical plane along the flume centerline (the subplots with the index 1) and along the middle of the contraction region, which is the region between the obstacle and channel wall (the subplots end with the index 2) for the obstacles a) cylinder, b) streamlined island, c) VSI, and d) RSI. The flow direction is from left to right for all subfigures.

Differing from the time-averaged kinematic variables, instantaneous velocity patterns exhibited temporally varying characters and presented clearer findings about the flow patterns in the wake region. From this perspective, in Figure 6, the instantaneous normalized streamwise velocities are presented in plan-view for the examined four characteristic obstacles. It is a fact from the literature that even two-dimensional bodies generate three-dimensional flow patterns in their wake region when they are exposed to flow. In other words, rear such 2D obstacles, the flow patterns near the bed and near the surface exhibit different characteristics. It should be noted that because of the three-dimensional geometry of RSI, this situation, i.e., variability of secondary flow pattern in the wake region along the depth, is expected to be more pronounced. According to this variability, instantaneous velocity patterns are presented in the wake region of RSI for both near the bottom (i.e., 5 cm away from the bed) and near the surface (i.e., 27 cm away from the bed). All the contour plots but RSI were prepared for the altitude of 27 cm, i.e., z/H=0.87, where z and H denote the altitude of the numerical probes and water depth, respectively.

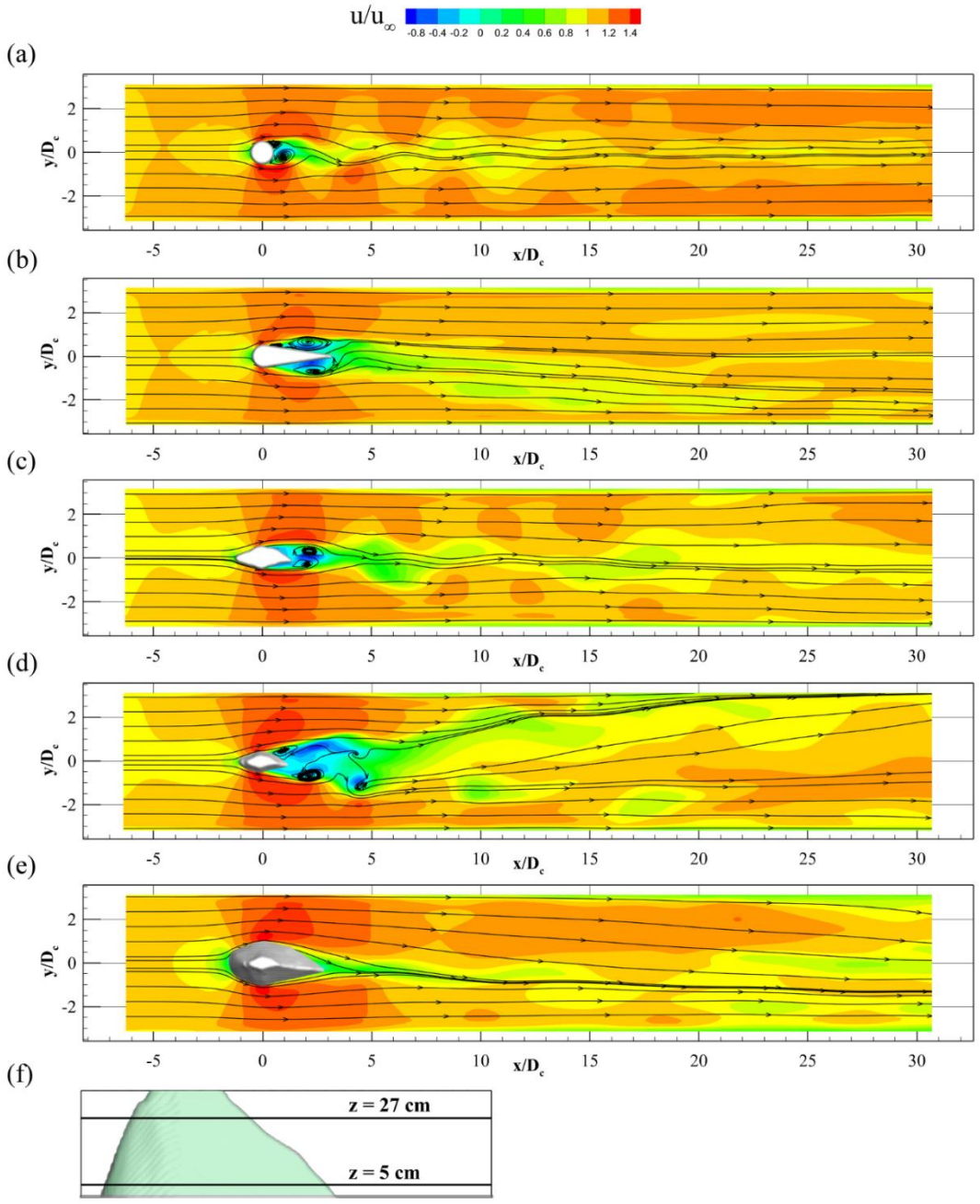

Fig. 6. Contour plots of instantaneous normalized streamwise velocities, u/U_∞, at the horizontal plane for the obstacles a) cylinder, b) streamlined island, c) VSI, d) RSI at the elevation of z=27 cm, and e) RSI at the elevation of z=5 cm. Subfigure f shows the elevations. The flow direction is from left to right for all subfigures.

The flow patterns (i.e., the red and green colors of the contour plots in Figure 6) that form behind the bodies were highly correlated with the forms of the obstacles. For instance, while the cylinder produced circular-shaped

secondary flow patterns, the streamlined island produced streamlined-like vortex-induced flow patterns. Among the others, the form of the streamlined island (Figure 6b) exhibited more hydrodynamic behavior against the flow than the other bodies. Due to the asymmetrical planform of the VSI and RSI cases (Figures 6c-6d), the large-scale von Karman vortex street gained more elongated and disorganized patterns compared to the cylinder case (Figure 6a). These complicated flow patterns observed in the wake region were attributed to the sharper angles at the edges of VSI and RSI, considering such unrounded bends are highly effective in terms of generating strong separation around the body.

Figures 6d and 6e show that the secondary flow structure was quite different for the RSI case due to this obstacle's vertically variable plan view. In the wake region, while well-defined pairs of vortices took place near the surface (Figure 6d), RSI acted against flow more like a streamlined body near the bed. The physical explanation behind this behavior can be the superposed impact of bed roughness and the RSI plan view elongation near the bed. More specifically, an increase in the turbulence near the bottom due to the bed roughness leads to a delay in separation, which is a well-documented fact for cylindrical obstacles (Sumer and Fredsøe, 1997). Besides, the combined impact of elongated cross-section near the bottom and inclined frontal slope of RSI provided a better hydrodynamic form to this obstacle which was similarly seen in the studies by Majd et al. (2016) and Kitsikoudis et al. (2017).

The propagation of the produced lee-wake vortices exhibited a quite dispersive character for RSI. Moreover, differing from the cylinder, for the RSI case, the separated vortices propagated asymmetrically towards the sides of the channel rather than remaining around the centerline of the flume. Therefore, in the downstream region of the RSI case, particularly at the sides of the channel, the velocities were dramatically different from each other.

Figure 7 shows the contour plots of the instantaneous normalized streamwise velocity patterns in the vertical plane along the flume centerline. Resultant vectors are also presented in the same figure to make the analysis more efficient. In these charts, sudden deceleration zones observed behind the bodies can be regarded as the natural outcome of intensive lee-wake vortices and turbulence-induced energy dissipation. While the form of the streamlined island produced a vertically identical velocity pattern, the flow structure behind the cylinder was highly variable along the depth. As can be seen in Figure 7a, due to the bed-generated flow turbulence, the onset of separation was delayed around the cylinder near the bottom. This implies a narrower wake region near the bottom than the near-surface for the cylinder case. This situation holds true for the VSI and RSI as well. The time-averaged streamwise velocity patterns presented in Figure 5 indicate a similar outcome. Therefore, in line with the previous studies (Roulund et al., 2005; Baykal et al., 2015; Ouro et al., 2017; Aksel et al., 2021), for these cases (cylinder, VSI, and RSI), the lee-wake vortices in the lower part of the obstacle were weaker than the upper part. Consequently, a quick recovery zone was observed near the bottom of the cylinder case.

As a result of its asymmetrical planform and the presence of unrounded bends on VSI, an intensive lee-wake vortex was detected behind this obstruction (Figure 7c). This situation is evident between 1.5-3.0 D_c, where D_c denotes the diameter of the cylinder. As stated previously, RSI produced vertically variable instantaneous streamwise velocity along the depth. Towards the depth, RSI gained a better hydrodynamic form against the incoming flow. More specifically, the planform view of the RSI near the bottom becomes more elongated (longer distance to generate a well-developed boundary layer) compared to the surface part of the RSI. This basic fact makes the flow kinematics highly variable around RSI along the depth. Also, a stronger contraction effect near the bottom (i.e., acceleration of flow and enhanced turbulence) at both sides of the obstacle is expected due to the enlargement of the cross-section.

Additionally, as in the cylinder case, presumably enhanced turbulence caused a delay in the onset of separation around the RSI near the bottom zone. Therefore, in the wake region of RSI, the strength of lee-wake vortices became weaker near the bed (Figure 5d1 and 5d2). The time-averaged streamwise velocity patterns for RSI show the same situation above (Figures 5d1 and 5d2). In other words, lee-wake vortices in the lower part of the RSI were weaker than in the upper part.

The difference between streamwise velocities of the contraction region (U_c) and wake region (U_w) induces a shear layer. The stronger shear brings the powerful lateral momentum transfer in the wake-field. Figure 8a1 displays the values of normalized streamwise velocity differences between contraction and wake region near the water surface (z=27 cm) in the vertical plane. Figure 8a2 shows the normalized streamwise velocity along the flume centerline at the same water level. The horizontal lines on both figures represent the length of obstacles on the channel bottom, and the inset figures show the side-view of the objects along the centerline. Streamwise velocities in the contraction and wake region of all examined obstacles were identical for the undisturbed flow on the upstream side. However, they exhibited different behavior in the wake zone because of the obstacle. Since the cylinder is not a streamlined object and can generate an adverse pressure gradient, there is severe deceleration behind it (Figure8a2). Figure 8 b1-b4 illustrates the relative locations of the velocities obtained relative to the obstacle, which allows assessing how fast the flow is recovering to the ambient flow.

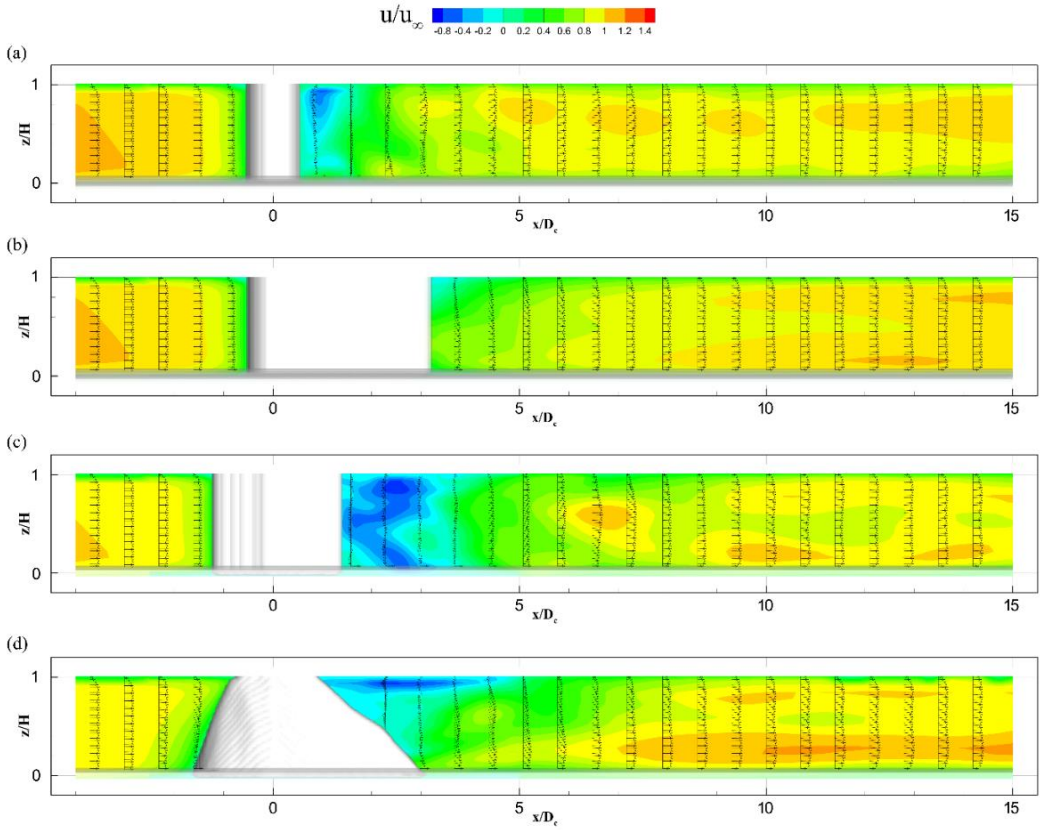

Fig. 7. The contour plots of the instantaneous normalized streamwise velocity patterns, u/U_∞, in the vertical plane along the flume centerline for a) cylinder, b) streamlined island, c) VSI, and d) RSI. The flow direction is from left to right for all subfigures.

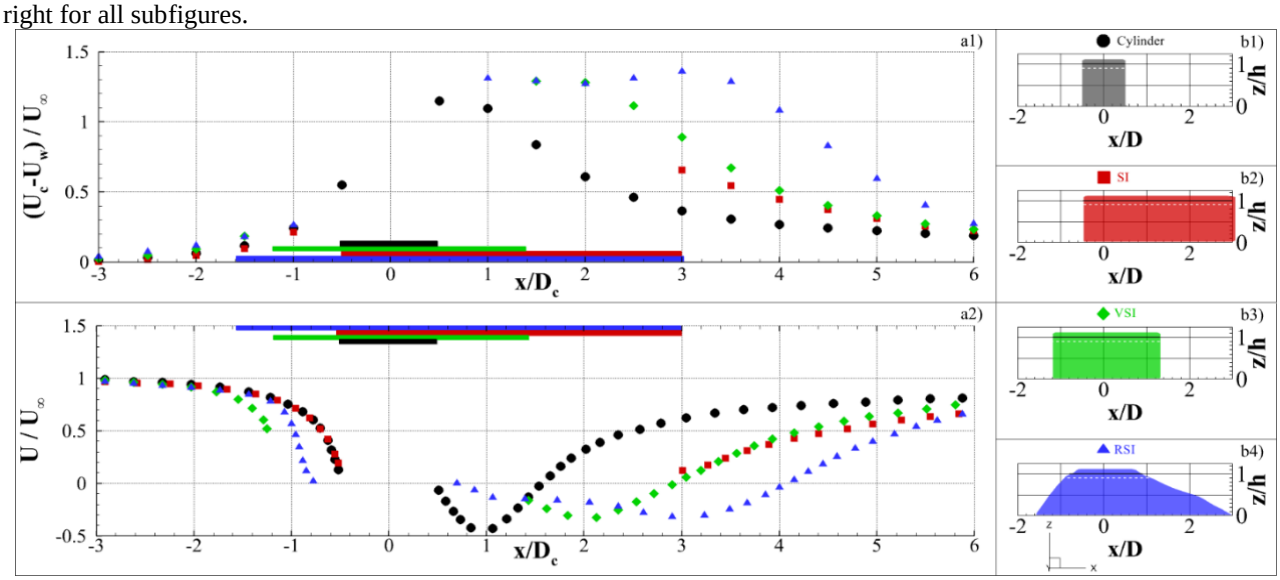

Fig. 8. a1) The difference between normalized streamwise velocities of contraction and wake region, $(U_c - U_w)/U_\infty$, and a2) Normalized streamwise velocities, u/U_∞, in the vertical plane at the elevation of z=27 cm. The side view of obstacles b1) cylinder, b2) streamlined island, b3) VSI, and b4) RSI in the flume centerline. The colored horizontal bars denote the actual location of the obstructions along the x/D axis. The dotted white lines on the insets (b1-b4) indicate the actual location of the velocities given on a1 and a2.

Consequently, quicker recovery was detected for the cylinder compared to the other examined obstacles due to stark shear-induced lateral momentum transfer (Figure 8a1). Also, the VSI produced a strong shear layer in its wake, like the cylinder, which recovered fast (Figure 8a1). The deceleration behind the VSI was pronounced, but it was less stark in comparison with the cylinder due to the body elongation (Figure 8a2). On the other hand, the streamlined island produced the weakest lateral momentum transfer due to a weaker shear layer (Figure 8a1), and its recovery was gradual (Figure 8a2). Figure 8a1 revealed a different pattern for the RSI case because of its slopes. It was seen that the value was growing stronger in the tail of the RSI, and it had a sudden decrease right after that. Nevertheless, in Figure 8a2, the flow deceleration recovery was gradually similar to the streamlined island in the RSI downstream.

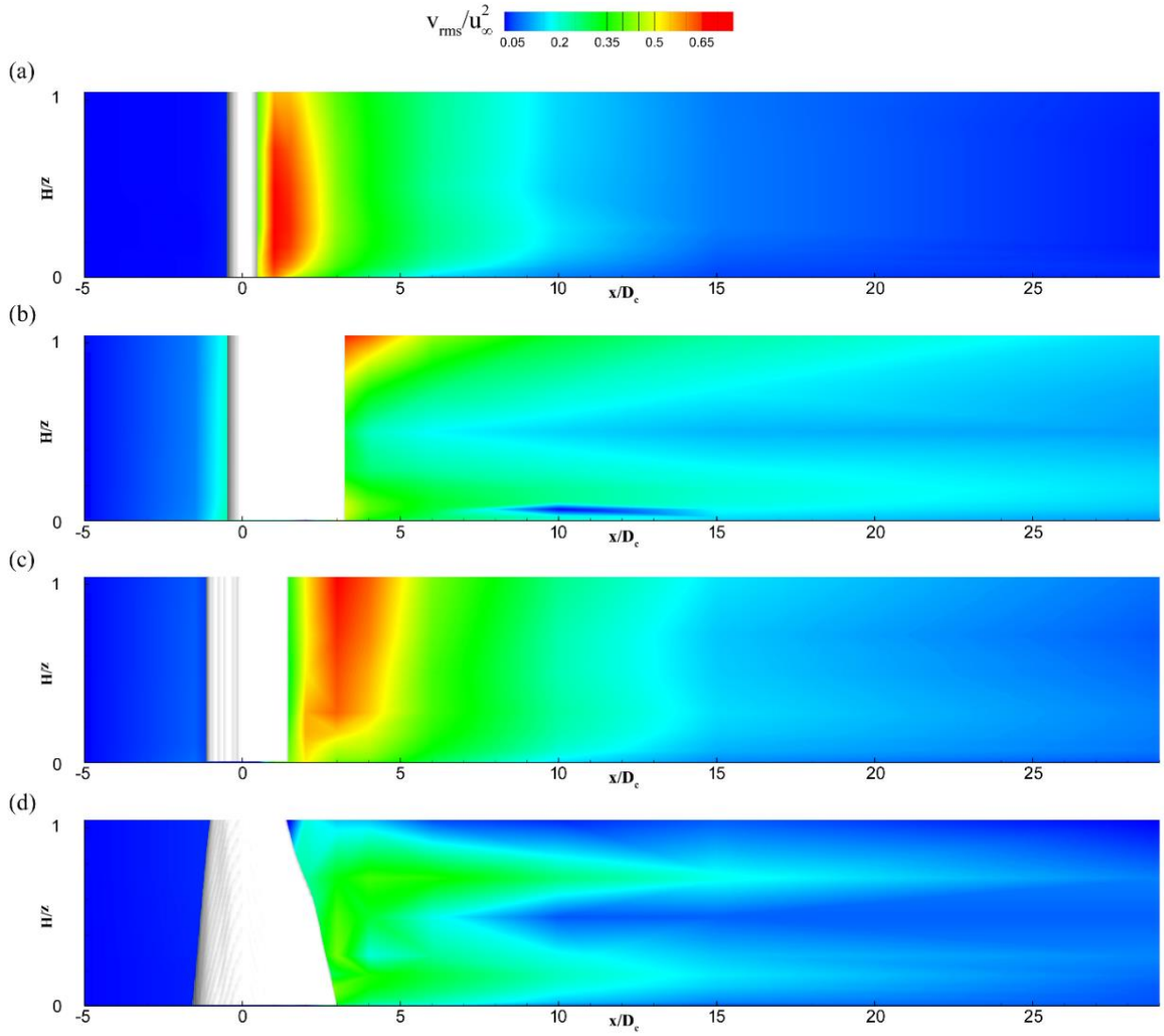

Fig. 9. The contour plots of the time-averaged normalized lateral turbulence intensity, v_{rms}/U_∞^2, patterns in the vertical plane along the flume centerline for a) cylinder, b) streamlined island, c) VSI, and d) RSI. The flow direction is from left to right for all subfigures.

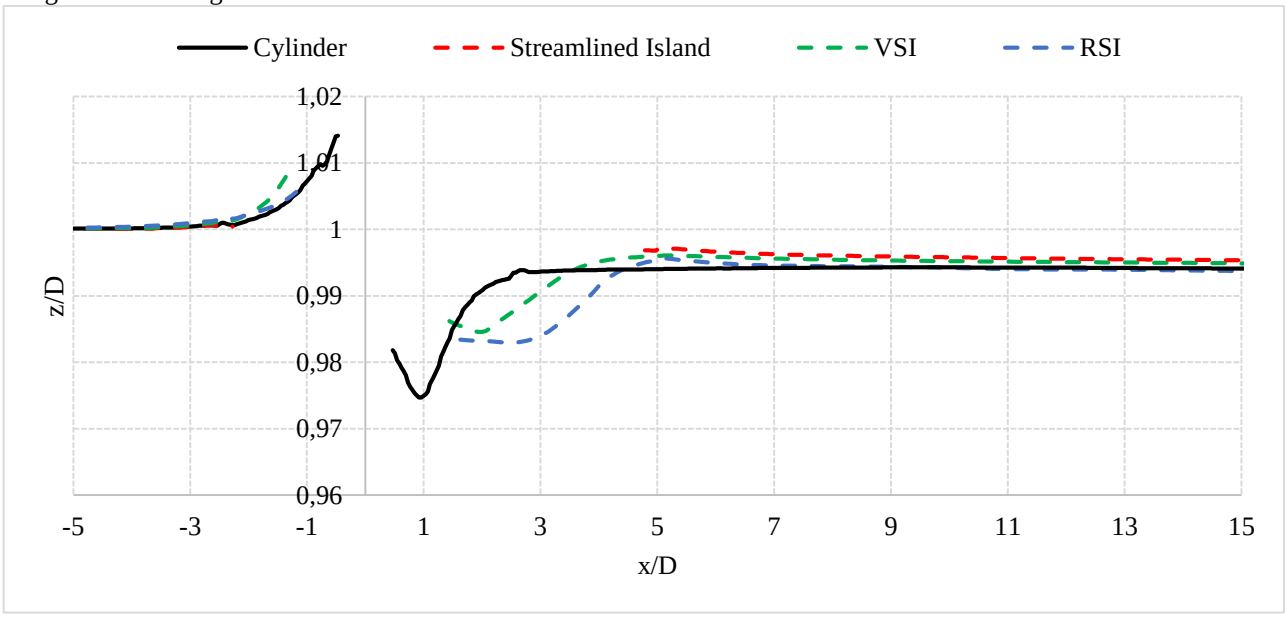

Fig. 10. The variation of time-averaged water surface levels along the centerline of the flume/obstacle for the case of the cylinder, streamlined island, VSI, and RSI.

Analysis of lateral turbulence intensity

It is obvious that the lateral turbulence intensity decreased in the region away from the bed. The pattern of this change depends on the form of the obstacle and the strength of the generated lee-wake vortices. However, towards the bed, the horseshoe vortex becomes an influential secondary flow structure in addition to lee-wake vortices that form around the bed. Therefore, the observed lateral intensity was the combined impact of these two energetic flow patterns, i.e., lee-wake vortices and horseshoe vortex. Hence, lateral turbulence intensity is a good indicator to quantify the strength of the generated pairs of vortices in the wake region. Based on this fact, Figure 9 shows the contour plots of the lateral turbulence intensity patterns in the vertical plane along the flume centerline.

It can be concluded that the behavior of the cylinder and VSI were similar to each other in terms of the strength of the produced vortices. Both of these obstacles (i.e., cylinder and VSI) generated severe vortices behind themselves. The presence of the stark vortices brought about shorter recovery distances for the cases of cylinder and VSI. Differing from these two cases, the recovery distances were markedly longer for streamlined island and RSI cases due to the absence of severe lee-wake vortices. This outcome also verifies that RSI is a streamlined obstacle form.

Boundary layer separation controls the flow pattern observed in the wake region of an obstacle. For a given Reynolds number, the body's geometry and the stagnation/depression levels at the front/rear sides of the body largely determine the development of this fundamental process. For the cylinder, the geometry greatly dictates the development of boundary layer separation along the depth. On the other hand, for a streamlined island, the difference between the stagnation/depression levels is the natural consequence of energy dissipation due to friction between water and the streamlined tail. This water level difference dictates the separation near the surface. The lateral momentum transfer in the wake region for the cylinder case is stronger than in the streamlined cases (VSI and RSI can also be regarded in this class) due to a distinct shear layer. This situation causes a quick recovery of the flow in the wake region, as shown in Figure 5a1. However, in the streamlined cases, the lack of a distinct shear layer causes less lateral mass transfer in the wake region and delays flow recovery, as seen previously in Figures 5 (b1, c1, and d1). In other words, the difference between the stagnation/depression levels at the upstream/downstream of the body is less affected due to the streamlined island form. These water levels that remain unchanged for long distances in the wake region (Figure 10) are particularly influential on the secondary flow structure near the surface region. This situation manifests itself as an enhanced lateral turbulence intensity only near the surface behind the streamlined island in Figure 9b.

Flow patterns around 2D and 3D islands

In Figure 11, the development of the secondary flow cells within the consecutive cross-sections (Figures 11a and 11b) are given for VSI and RSI. It can be deduced that RSI had a higher ability to produce organized secondary flow patterns than VSI. Furthermore, RSI produced large-scale counter-rotating streamwise vortices (LSCSVs) with three cells downstream of the cross-section (Figure 11l). The cell near the bottom rose, broke into two smaller pieces, and contributed to the existing two cells near the water surface.

In Figure 12, the progression of velocity profiles around VSI and RSI is given to directly compare the lateral distribution of normalized streamwise velocity profiles around the obstacles. For VSI and RSI, the development of lateral distributions of velocity profiles is compared for identical elevations. The onset of separation forms earlier and more significantly for VSI (Figure 11a) compared to RSI (Figure 12c) at the same water level. It can be regarded that this situation is due to the clear manifestation that VSI has a less hydrodynamic form than RSI. During the analysis, it was also assumed that the primary reason behind this situation could be the strength of turbulence around those objects. Indeed, when the turbulence kinetic energies (TKE) were examined (Figure 12b, 12d, and 12f), it was seen that there was a strong correlation between the delay in onset of separation and the magnitude of TKE. Therefore, in the RSI case near the bed, excessive turbulence prevents separation behind the body.

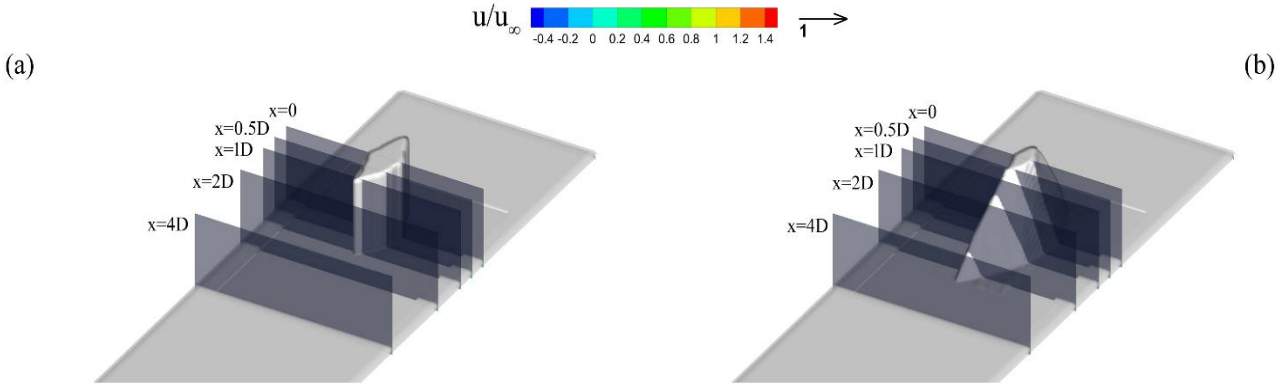

Fig. 11. Demonstration of the progression of secondary flow cells in the streamwise direction by means of taking consecutive cross-sections downstream (a) VSI and (b) RSI obstacles, at distinct distances.

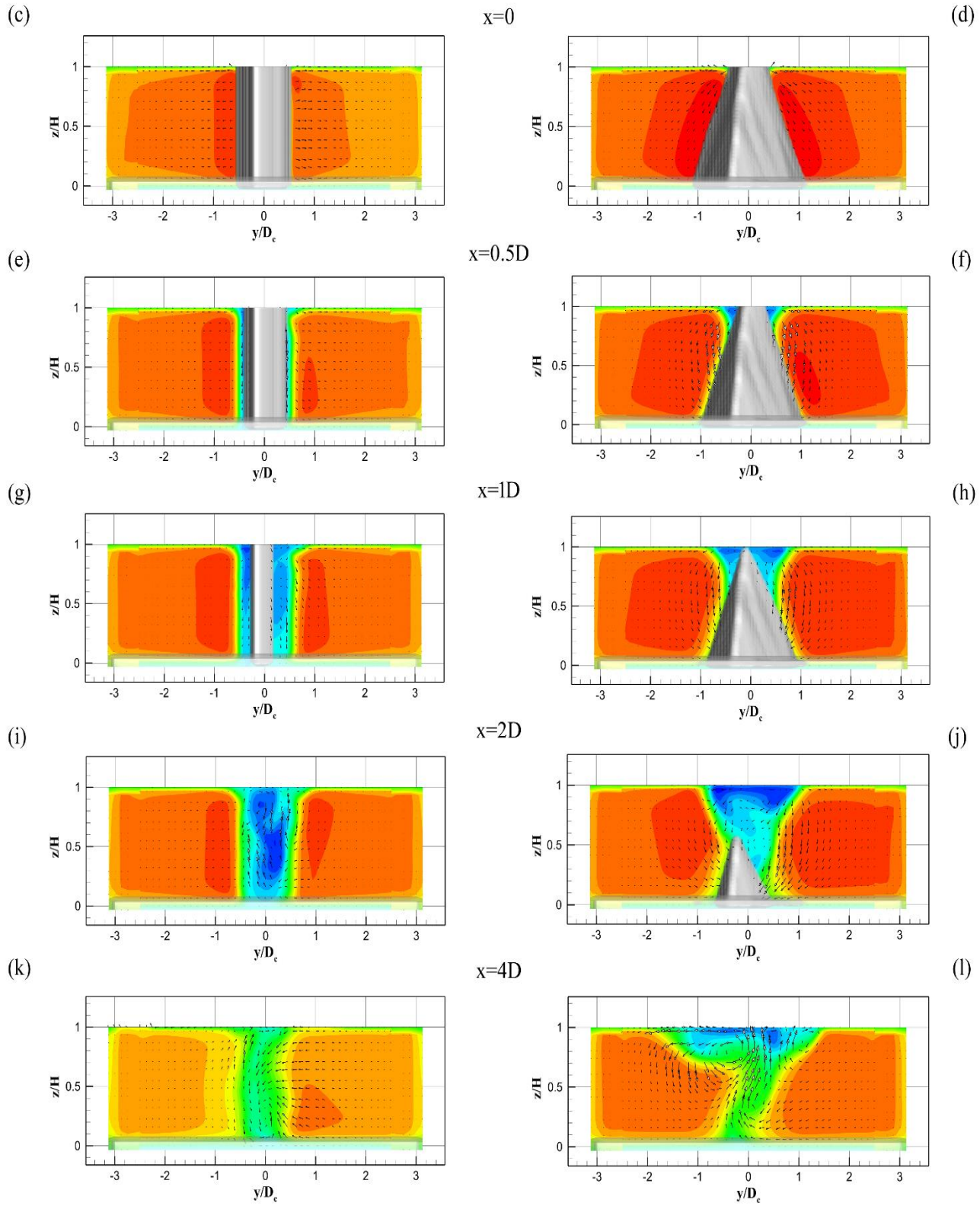

Fig. 11 (cont.). Demonstration of the progression of secondary flow cells in the streamwise direction by means of taking consecutive cross-sections downstream (a) VSI and (b) RSI obstacles, at distinct distances. Contour maps of the mean local flow relative to the ambient flow for the VSI at a downstream distance of: (c) x=0, (e) x=0.5, (g) x=1, (i) x=2, (k) x=4, and for the RSI at a downstream distance of: (d) x=0, (f) x=0.5, (h) x=1, (j) x=2, (l) x=4.

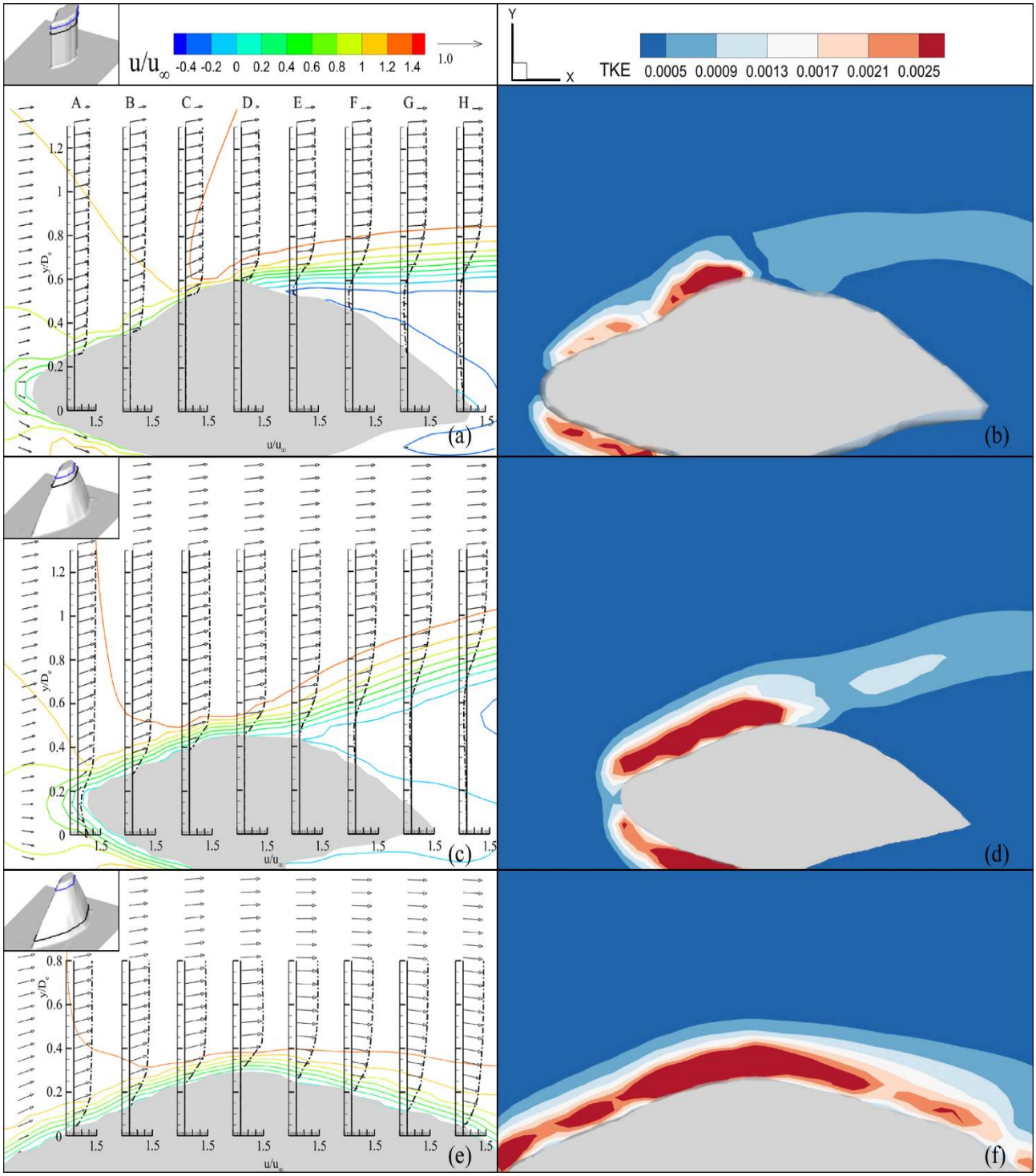

Fig. 12. Progression of instantaneous velocity profiles around a) VSI and c, e) RSI. Turbulent kinetic energies (TKE) around b) VSI and d, f) RSI. The insets' black lines denote the horizontal plane's elevation, where the lateral distribution of normalized streamwise velocity profiles is generated. The blues lines in the insets indicate the still water surface levels around the islands. The resultant vectors were calculated based on the streamwise and lateral velocity components.

Analysis of bed shear stress

The variation of normalized time-averaged bed shear stress for the examined obstacles is given in Figure 13. During the normalization, undisturbed bed shear stress was used. In line with previous findings, while the streamlined island generated the least bed shear stress, the cylinder produced the greatest values. When the case of RSI was considered, it was seen that the side slopes of the RSI were exposed to the highest bed-shear stress. Besides, the flow applied lower bed shear stress to the island's tail. Furthermore, relatively high bed shear stress was observed where the island slopes intersect with the bottom.

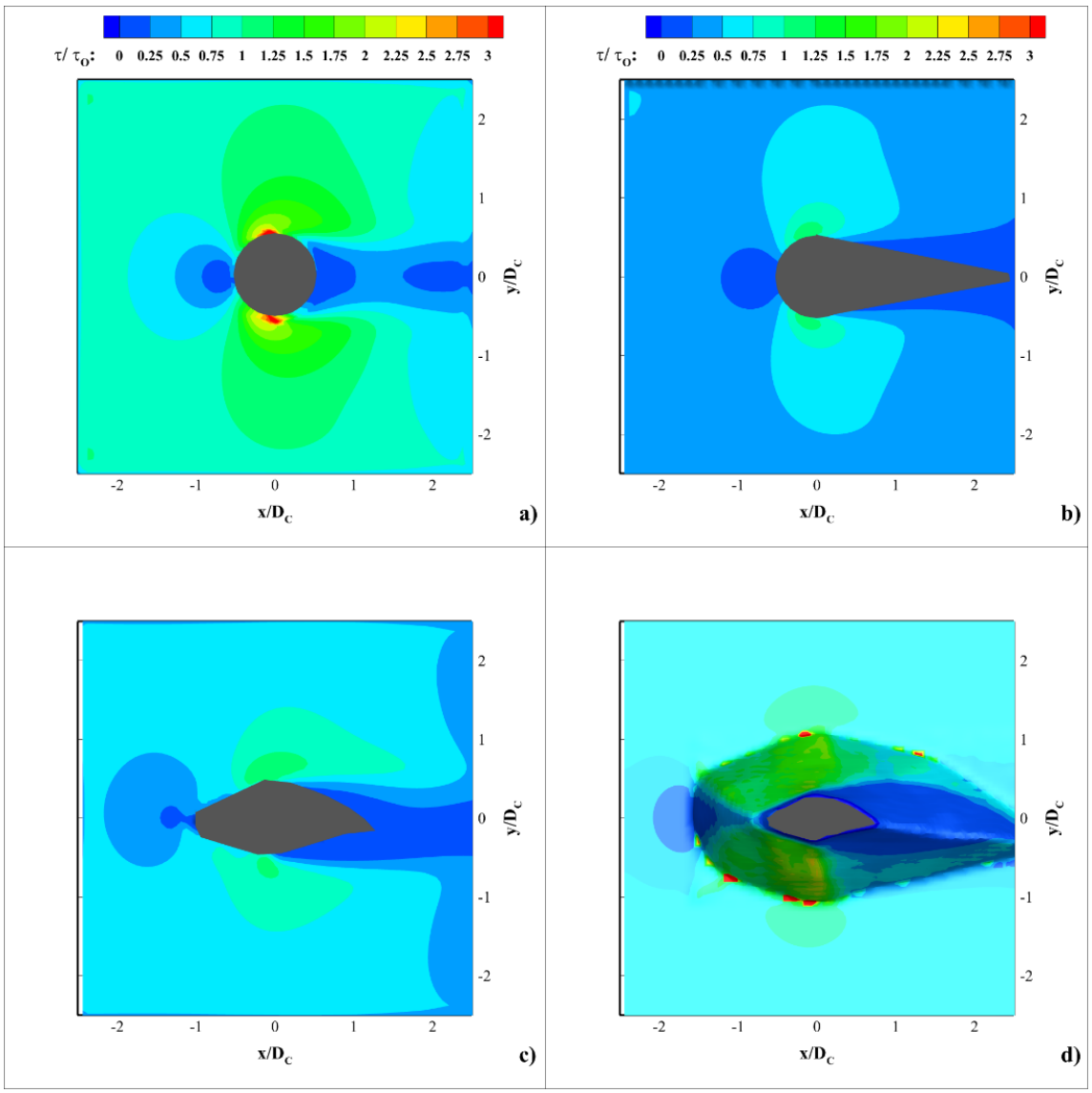

Fig. 13. The normalized time-averaged bed shear stress, τ/τ_0, variation for a) cylinder, b) streamlined island, c) VSI, and d) RSI. The flow direction is from left to right for all subfigures.

Discussion

The primary aim of this study was to comprehend the flow patterns around an island-like geometry with a 3D form (i.e., RSI). It is evident from the pertinent literature that even 2D bodies exposed to the flow overwhelmingly generate 3D flow patterns around themselves. To present a complete analysis regarding flow around an island form, the flow patterns around 2D bodies, i.e., cylinder and streamlined island, were simulated in the study as well-known reference cases. As a starting point, such a comparative method facilitated a better understanding of the contribution of the island's three-dimensionality to the generated flow patterns. The underlying motivation behind understanding the observed secondary flow was that these flow patterns might underpin the generation of a well-functioning river system. This section presents a synthesis between secondary flow patterns and their possible ecological services in the riverine process, and the limits of the present work are highlighted.

According to the numerical results, VSI and RSI created elongated von Karman vortex streets with a disorganized distribution of vortices in their wake region. This situation implies that with their perturbative effects, MCIs may be capable of triggering the meandering process in lowland rivers. Furthermore, straightened rivers with trapezoidal channels have a homogeneous physical habitat and reduced eco-diversity (Brookes, 1994). Therefore, it is plausible that midchannel islands may provide eco-services by enhancing meandering processes in natural waterways. The crucial role of the meandering process in the creation of cross-sectional heterogeneity-induced bio-diversity was documented by the restoring programs applied in many regions as stated by Nakano and Nakamura (2008), i.e., in the USA (Toth et al., 1993), Europe (Holmes, 1998), and Japan (Nakamura, 2003). Besides, the study by Nakano and Nakamura (2008) pointed out that a shallow, stable riverbed due to helical flow in meandering waterways generates a suitable habitat for macroinvertebrates in lowland rivers.

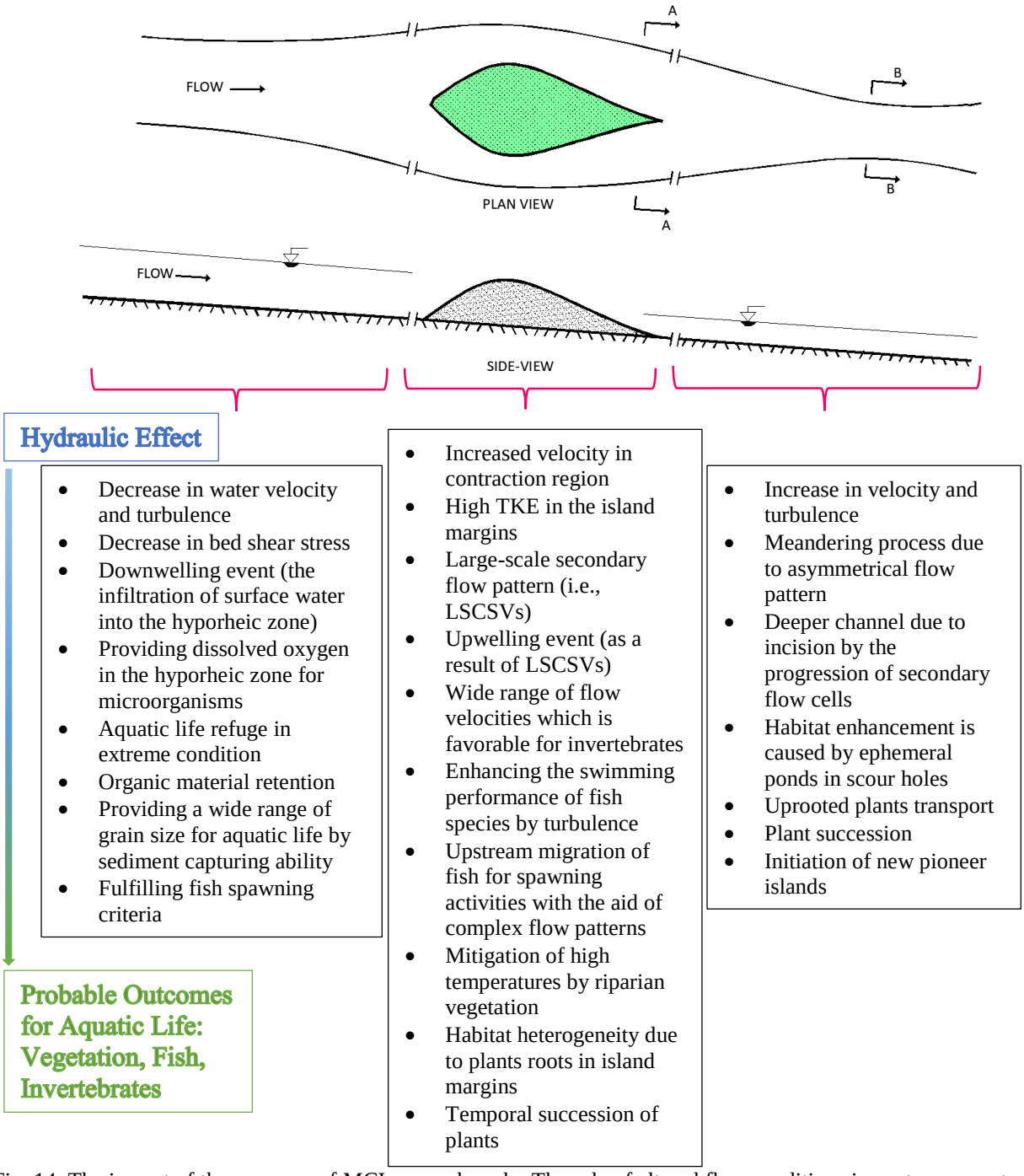

Fig. 14. The impact of the presence of MCI on reach scale: The role of altered flow conditions in upstream, contraction, and downstream zones.

In general, the localized variations in velocity, turbulence, and bed shear stress in the wake region of the in-stream obstructions lead to the accumulation of sediment depositions and produce suitable conditions for the reproduction of vegetation in these sediment deposits (Yagci and Strom, 2022). Furthermore, colonization of vegetation patches and their diverse adaptation to aquatic environments increase the plants' durability in submersion and water deficiency periods (Corenblit et al., 2015). Consequently, the regenerated riparian plant biomes in river corridors increase the bank/floodplain stability due to soil reinforcement by their roots (Abernethy and Rutherfurd, 1999; Hubble et al., 2010), promote the ecological stability (Naiman et al., 1993), improve the quality of water (Skłodowski et al., 2014), and enhance the flow variability within the cross-section (Valyrakis et al., 2021).

The findings indicated that an MCI generates flow divergence. It also increases the velocity in the contraction region. Hence, the MCI becomes elongated by transporting the sediment and woody debris to its lee side. The strong resilience of some plant species in high velocities and destructive flows, e.g., *Salix*, *Populus*, and *Alnus* (Francis et al., 2009), leads to vegetation regrowth and island expansion (Corenblit et al., 2009). This mechanism increases the MCI endurance in channel migration or degradation by flood events (Gurnell et al.,

2001). The MCI enlargement generates ephemeral ponds in scour holes which causes habitat enhancement on an individual scale and reach scale (Gurnell et al., 2005). Furthermore, the high TKE in the margins of MCI may entrain the submerged plants on the island edge. These uprooted plants can have positive feedback on biodiversity by both organic material retention (Gurnell et al., 2012) and plant succession within the initiation of pioneer islands downstream of the island (Francis et al., 2009).

One of the crucial findings was that MCI generates significant secondary flow in the wake region. This alteration in flow structure due to natural in-stream obstructions may have great potential in terms of enhancing the riverine ecology by directly influencing fish and invertebrates (Bunn and Arthington, 2002). Fish spawning requires a wide range of sediment characteristics (Moir et al., 2002), and the flow patterns around MCIs may prepare a substrate with an appropriate grain size distribution for fish assemblage. Also, the various grain sizes provided by midchannel bars (Ashworth, 1996) are advantageous for aquatic macroinvertebrates, which are the main food source for many fish species (Nie, 1987). Moreover, the plant roots near the banks increase habitat heterogeneity and lead to an abundance of invertebrates (Beisel, 1998). The wide range of flow velocities generated by the presence of MCIs is very suitable for these organisms (Jowett and Richardson, 1990) due to their inherent need and high tolerance (Hynes, 1970; Minshall, 1984). Temperature plays an important role in the growth, survival and spawning of fresh water fish species (Zhang et al., 2021). Consequently, the thermal extremes in the rivers affect their breeding success. All cold-water fish species stop growing when the water temperature rises above 20°C and increasing the water temperature is lethal during fish spawning and migration (Bell, 1991). Both coarse sediment (Ock et al., 2015) and vegetation (Hannah et al., 2004; Ryan et al., 2013; Garner et al., 2014) of midchannel bars mitigate the temperature extremes, especially in summer peaks. The effect of temperature reduction by riparian vegetation is more pronounced in the areas with low flow velocity due to higher residence time (Garner et al., 2017). Therefore, the upstream area of the MCI can be a proper refugium in extreme conditions and fulfill the criteria for fish spawning activities. On the other hand, the wake zone with complex flow patterns helps their upstream migration (Hinch and Rand, 1998; McLaughlin and Noakes, 1998). Many researchers (e.g., Boisclair and Tang, 1993; Lupandin, 2005; Liao et al., 2013; Smith et al., 2014) suggested that turbulence can enhance the swimming performance of the fish.

Figures 5, 6, 7, and 9 showed that streamlined bodies are highly productive in generating pronounced large-scale secondary flow patterns. These secondary flow patterns (i.e., LSCSVs) may adjust river bottom morphology (i.e., channel incision), as previously demonstrated by Heidari et al. (2021). The LSCSVs in island wake improve the vertical exchange of water (Chang et al., 2013a). The nutrient-rich deep subsurface water is brought to surface water by upwelling in the wake region (Heywood et al., 1990; Coutis and Middleton, 1999). According to Corenblit et al. (2015), plants' temporal succession occurs parallel with the vertical exchange of surface and subsurface water. In addition, downwelling events upstream of the island infiltrate oxygen-rich water into the riverbed sediment (Boulton et al. 1998; Baxter et al. 2003), which is advantageous for invertebrates by providing dissolved oxygen (DO) in the hyporheic zone (Maazouzi et al., 2013). Also, the interaction between downwelling and upwelling zones brings about ecological productivity (Dent et al. 2001), and the elongated wake zone in the RSI provides remarkable eco-services in the riverine environment. Due to these beneficial ecological services, it is recommended that practitioners conserve the midchannel islands, which were traditionally regarded as a source of undesirable hydraulic resistance in river restoration projects. Figure 14 represents the impact of the island presence on a river reach from hydraulic to ecological context.

This study was undertaken only for a specific Reynolds number (Re=52800) and the numerical channel's width-to-depth ratios (W/H). Different Re and W/H influence the secondary flow patterns to some extent. Hence, the presented numerical results can help to explain the hydrodynamics behind midchannel islands to a certain degree. Further investigation on the role of Re and W/H on secondary flow patterns rear the MCIs is recommended. Also, changing the island shape, frontal/rear slopes, and elongation ratio can lead to slightly different results. It should be borne in mind that the primary aim of this modeling study was to capture only the major secondary flow structure that emerges around a typical island form. In future studies, more sophisticated numerical models with temporally/spatially higher resolution (e.g., LES or DNS) should be run to analyze the flow patterns with finer scales.

It is also worth highlighting that the methodology was adopted in the present numerical study, not to be confused with a scaled numerical study (the model was calibrated based on experimental data, not field data). The numerical simulations are directed towards understanding the hydrodynamic processes around a midchannel island. The study aimed to identify the influence of the geometrical form of this arbitrarily chosen representative island on generated flow patterns within the traditional fluid mechanics perspective. This analysis was carried out comparatively by benefiting from the existing knowledge extracted from well-known reference cases (i.e., cylinder and streamlined island). These bodies were simulated under the same numerical model, and the obtained outcomes provided a base for the comparative analysis. Since the island was arbitrarily chosen from satellite observations and the model was calibrated based on flume experiments rather than field data, it is intentionally avoided to develop an empirical equation, considering such an equation may misdirect practitioners who work in the river management field. It should also be remembered that the model outputs presented in this study are inevitably under a scale effect since the model calibration was undertaken based on the flume experiments. In fact, perfect scaling-down is not practically possible in

numerical and physical models because of the inability to keep each relevant force ratio constant between the scaled and real-world models. However, scaling up this study's results could be attempted considering Froude's similarity of the proper flow and geometric parameters (Hughes, 1993; Heller, 2011).

As aforementioned, the island shape controls the flow in its wake region and ecohydrological processes in a natural river system (Heidari et al., 2021). According to Wyrick and Klingeman (2010), islands are categorized into three primary forms: (1) streamlined, (2) angular, and (3) irregular, and these forms can refer to the island age. The typical island form, exposed to high flows for a long time, tends to be more streamlined (Collier et al., 2015). Our numerical outputs revealed that the examined RSI exhibited a streamlined hydrodynamic behavior. The generated secondary flow patterns observed in the wake region of such islands are sensitive to many variables, i.e., island form, Reynolds number, contraction ratio, sediment/vegetation texture distribution on the island/riverbed, and channel bottom gradient. Because of this complexity, generating an empirical formula or presenting a quantitative analysis for the flow patterns rear the MCI (i.e., RSI) was kept beyond the scope of this work. Instead, we aimed to understand only the influence of geometric characteristics of the island on the major secondary flow patterns and to synthesize the probable ecological consequences considering that such knowledge may constitute a background for river restoration projects. It is recommended for future studies to examine further the role of other variables mentioned above on flow characteristics in the wake of MCI.

Conclusion

A numerical study investigated the flow structure behind an island-like geometry. To investigate the interaction between flow and midchannel islands and understand their three-dimensionality role in the flow domain, flow around 2D bodies was first simulated. After the validation/calibration process, the model was implemented for the RSI, which has a 3D form. The following conclusions were attained from this study.

1) Spatial variation of various kinematic variables indicated that RSI is a streamlined obstacle. Therefore, it exhibited certain similarities with the streamlined island in terms of flow structure in the wake region. As in a streamlined island, RSI generated relatively weaker lee-wake vortices that bring about gradual recovery.
2) Towards the bed, RSI gained more hydrodynamic form against the flow due to the elongation of its plan view. Besides, contraction-induced acceleration in the strength of flow and enhancement in bed shear stress delayed the onset of separation near the bed. It was also observed that there was a high correlation between the magnitude of TKE and the delay in boundary layer separation around the RSI.
3) Simulations indicated that, differing from the other 2D obstacles (i.e., cylinder, streamlined island, and VSI), RSI produced highly variable flow patterns along with the depth. For the RSI, while well-defined pairs of vortices were monitored near the water surface, streamlined behavior against the flow was observed near the bed.
4) It was seen that because of the asymmetrical planform of RSI, the produced pairs of vortices exhibited elongated and disorganized distribution in the wake region. In addition, these vortices, separated from the boundary layer, propagated asymmetrically towards the sides of the active channel rather than remaining around the centerline of the flume.
5) When the findings from the numerical model and the knowledge from the pertinent literature were evaluated together, it was concluded that midchannel islands might have a significant eco-geomorphological function. Furthermore, with their perturbative effect on the flow field (e.g., spatial flow variability in the active channel, generation of large-scale secondary flow patterns, lateral and vertical mixing, production of helical flow), MCIs can provide countless ecomorphological services (e.g., supporting habitat for macroinvertebrates, preparing the substrate with an appropriate grain size distribution for fish assemblage, regeneration of vegetation patches from living driftwood deposited in sediment mound in the wake region, and enhancing biodiversity). Therefore, it is recommended that midchannel islands, which are traditionally regarded as additional hydraulic resistance, should be preserved in river restoration projects within the ecological engineering perspective to create living and ecological well-functioning river systems.

Acknowledgment

The support of the HEC ENGINEERING is gratefully acknowledged.

References

Abernathy, B., Rutherford, I.D. (1999). Guidelines for stabilizing streambanks with riparian vegetation. Technical Report 99/10, Cooperative Research Centre for Catchment Hydrology, Parkville, Victoria, 30 pp.

Aksel, M., Yagci, O., Kirca, V.S.O., Erdog, E., Heidari, N. (2021). A comparative analysis of coherent structures around a pile over rigid-bed and scoured-bottom. *Ocean Eng.*, 226, 108759. doi.10.1016/j.oceaneng.2021.108759.

Ashmore, P.E. (1993). Anabranch confluence kinetics and sedimentation processes in gravel-braided streams. In *Braided Rivers*, Best, J. L., Bristow, C.S., eds., Geological Society, London, Special Publication, 75, 129-146. doi.10.1144/GSL.SP.1993.075.01.08.

Ashworth, P.J. (1996). Mid-channel bar growth and its relationship to local flow strength and direction. *Earth Surf. Process. Landforms*, v. 21, 103–123.

Ashworth, P.J., Best, J.L., Roden, J.E., Bristow, C.S., Klaassen, G.J. (2000). Morphological evolution and dynamics of a large, sand braid-bar, Jamuna River, Bangladesh. *Sedimentology*, 47(3), 533–555. doi.1046/j.1365-3091.2000.00305.x

Baxter, C., Hauer, F.R., Woessner, W.W. (2003). Measuring groundwater–stream water exchange: new techniques for installing minipiezometers and estimating hydraulic conductivity. *T. Am. Fish. Soc*., 132, 493–502.

Baykal, C., Sumer, B.M., Fuhrman, D.R., Jacobsen, N.G., Fredsøe, J. (2015). Numerical investigation of flow and scour around a vertical circular cylinder. *Phil. Trans. R. Soc.*, A 373 (2033), 20140104. doi.10.1098/rsta.2014.0104.

Beisel, J., Usseglio-Polatera, P., Thomas, S., Moreteau J.C. (1998). Stream community structure in relation to spatial variation: the influence of mesohabitat characteristics. *Hydrobiologia*, 389, 73–88. doi.10.1023/A:1003519429979.

Bell, M.C. (1991). Fisheries Handbook of Engineering Requirements and Biological Criteria. Fish Passage Development and Evaluation Program, Corps of Engineers, North Pacific Division, Portland, Oregon, 322 pp.

Bennett, S., Wu W., Alonso, C.V., Wang, S.Y. (2008). Modeling fluvial response to in-stream woody vegetation: Implications for stream corridor restoration. *Earth Surf. Process. Landforms*, 33(6), 890–909. doi.10.1002/esp.1581.

Boisclair, C.D. Tang, M. (1993). Empirical analysis of the influence of swimming pattern on the net energetic cost of swimming in fishes. *J. Fish Biol.*, 42:183. doi.10.1111/j.1095-8649.1993.tb00319.x.

Boulton, A.J. Foster, J.G. (1998). Effects of buried leaf litter and vertical hydrologic exchange on hyporheic water chemistry and fauna in a gravel-bed river in northern New South Wales, Australia. *Freshwater Biol.*, 40, 229–243. doi.10.1046/j.1365-2427.1998.00345.x.

Brierley, G.J., Fryirs, K.A. (2005). Geomorphology and River Management: Applications of the River Styles Framework. 398 pp., Blackwell, Malden, Mass.

Brookes, A. (1994). River channel change. In *The Rivers Handbook*, Volume 2, Calow, P., Petts. G., eds., Blackwell: Oxford, 55–75.

Bunn, S.E., Arthington, A.H. (2002). Basic Principles and Ecological Consequences of Altered Flow Regimes for Aquatic Biodiversity. *Environ. Manag.*, 30, 492–507. doi.10.1007/s00267-002-2737-0.

Callow, J.N., Smettem, K.R.J. (2007). Channel response to a new hydrological regime in southwestern Australia. *Geomorphology*, 84(3–4), 254–276. doi.10.1016/j.geomorph.2006.01.043.

Carson, M.A. (1984). The meandering-braided river threshold: a reappraisal. *J. Hydrol.*, 73, 315– 334. doi.10.1016/0022-1694(84)90006-4.

Chang, M.-H., Tang, T.Y., Ho, C.-R., Chao, S.-Y. (2013a). Kuroshio-induced wake in the lee of Green Island off Taiwan. *J. Geophys. Res. Oceans*, 118, 1508–1519. doi. 10.1002/jgrc.20151.

Chang, W.Y., Constantinescu, G., Lien, H.G., Tsai, W.F., Lai, J.S., Loh, C.H. (2013b). Flow structure and sediment entrainment mechanisms around bridge piers of varying geometrical complexity. *J. Hydraul. Eng.*, 812–826. doi.10.1061/(ASCE)HY.1943-7900.0000742.

Collier, J.S., Oggioni, F., Gupta, S., Moreno, D.G., Trentesaux, A., Batist M.De. (2015), Streamlined islands and the English Channel megaflood hypothesis. *Global Planet. Change*, 135, 190–206. doi.10.1016/j.gloplacha.2015.11.004.

Corenblit, D., Davies, N.S., Steiger, J., Gibling, M.R., Bornette, G. (2015). Considering river structure and stability in the light of evolution: feedbacks between riparian vegetation and hydrogeomorphology. *Earth Surf. Process. Landforms*, 40, 189–207. doi.10.1002/esp.3643.

Corenblit, D., Steiger, J., Gurnell, A.M., Tabacchi, E., Roques, L. (2009). Control of sediment dynamics by vegetation as a key function driving biogeomorphic succession within fluvial corridors. *Earth Surf. Process. Landforms*, 34(13), 1790–1810. doi.10.1002/esp.1876.

Coutis, P.F. Middleton J.H. (1999). Flow-topography interaction in the vicinity of an isolated, deep ocean island. *Deep Sea Res. I*, 46(9), 1633–1652. doi.10.1016/S0967-0637(99)00007-2.

Dent, C.L., Grimm, N.B., Fisher, S.G. (2001) Multiscale effects of surface–subsurface exchange on stream water nutrient concentrations. *J. N. Am. Bentholl. Soc.*, 20,162–181. doi.10.2307/1468313.

Edwards, P.J., Kollmann, J., Gurnell, A.M., Petts, G.E., Tockner K., Ward J.V. (1999). A conceptual model of vegetation dynamics on gravel bars of a large Alpine River. *Wetl. Ecol. Manag.*, 7, 141–153. doi.10.1023/A:1008411311774.

Eekhout, J.P.C., Hoitink, A.J.F., Mosselman, E. (2013). Field experiment on alternate bar development in a straight sand-bed stream. *Water Resour. Res.*, 49, 8357–8369. doi.10.1002/2013WR014259.

Euler, T., Zemke, J., Rodrigues, S., Herget, J. (2014). Influence of inclination and permeability of solitary woody riparian plants on local hydraulic and sedimentary processes. *Hydrol. Process.*, 28(3), 1358–1371. doi.10.1002/hyp.9655.

Flowscience. (2019). Flow-3D User Manual.

Francis R.A. (2006). Allogenic and autogenic influences upon riparian vegetation dynamics. *Area*, 38, 453–464. doi.10.1111/j.1475-4762.2006.00706.x.

Francis, R.A., Corenblit, D. Edwards, P.J. (2009). Perspectives on biogeomorphology, ecosystem engineering and self-organization in island-braided fluvial ecosystems. *Aquat. Sci.*, 71, 290. doi.10.1007/s00027-009-9182-6.

Garner, G., Malcolm, I.A., Sadler, J.P., and Hannah, D.M. (2017). The role of riparian vegetation density, channel orientation and water velocity in determining river temperature dynamics. *J. Hydrol.*, 553, 471-485. doi.10.1016/j.jhydrol.2017.03.024.

Garner, G., Malcolm, I.A., Sadler, J.P., Hannah, D.M., (2014). What causes cooling water temperature gradients in a forested stream reach? *Hydrol. Earth Syst. Sci.*, 18(12), 5361–5376. doi.10.5194/hess-18-5361-2014.

Guo, B., Ahmadian, R., Evans, P., Falconer, R.A. (2020). Studying the Wake of an Island in a Macro-tidal Estuary. *Water*, 12(5), 1225. doi.10.3390/w12051225.

Gurnell, A.M., Petts, G.E. (2002) Island-dominated landscapes of large floodplain rivers, a European

perspective. *Freshw. Biol.*, 47, 581–600. doi.10.1046/j.1365-2427.2002.00923.x.

Gurnell, A.M., Bertoldi, W., Corenblit, D. (2012). Changing River channels: The roles of hydrological processes, plants and pioneer fluvial landforms in humid temperate, mixed load, gravel bed rivers. *Earth Sci. Rev.*, 111, 129–141. doi.10.1016/ j.earscirev.2011.11.005.

Gurnell, A.M., Petts, G.E., Hannah, D.M., Smith, B.P.G., Edwards, P.J., Kollmann, J., Ward, J.V., Tockner, K. (2001). Riparian vegetation and island formation along the gravel-bed Fiume Tagliamento, Italy. *Earth Surf. Process. Landforms*, 26 (1), 31–62. doi.10.1002/1096-9837(200101)26:1<31::AID-ESP155>3.0.CO;2-Y

Gurnell, A.M., Tockner, K., Edwards, P.J., Petts, G.E. (2005). Effects of deposited wood on biocomplexity of river corridors. *Front. Ecol. Environ.*, 3(7), 377–382. doi.10.1890/1540-9295(2005)003[0377:EODWOB]2.0.CO;2.

Hannah, D.M., Malcolm, I.A., Soulsby, C., Youngson, A.F. (2004). Heat exchanges and temperatures within a salmon spawning stream in the Cairngorms, Scotland: seasonal and sub-seasonal dynamics. *River Res. Appl.*, 20(6), 635–652. doi.10.1002/rra.771.

Heidari, N., Yagci, O., Aksel, M. (2021). Midchannel islands in lowland river corridors and their impacts on flow structure and morphology: A numerical based conceptual analysis. *Ecol. Eng.*, 173, 106419, doi.10.1016/j.ecoleng.2021.106419.

Heller, V. (2011). Scale effects in physical hydraulic engineering models. *J. Hydraul. Res.*, 49(3), 293–306. doi.10.1080/00221686.2011.578914.

Heywood, K.J., Barton, E.D., and Simpson J.H. (1990). The effects of flow disturbance by an oceanic island. *J. Mar. Res.*, 48, 55–73. doi.10.1357/ 002224090784984623.

Hinch, S. G., Rand, P.S. (1998). Swim speeds and energy use of upriver-migrating sockeye salmon (Oncorhynchus nerka): role of local environment and fish characteristics. *Can. J. Fish. Aquat. Sci.*, 55,1821–1831 (1998). doi.10.1139/f98-067.

Holmes N.T.H. (1998). The river restoration project and its demonstration reaches. In *Rehabilitation of Rivers*, Waal, L. C., Large, A. R. G., Wade, P. M., eds., Wiley: New York, 133–148.

Hooke, J. M. (1986). The significance of mid-channel bars in an active meandering river. *Sedimentology*, 33, 839–850. doi.10.1111/j.1365-3091.1986.tb00986.x.

Hubble, T.C.T., Docker, B.B., Rutherfurd, I.D. (2010). The role of riparian trees in maintaining riverbank stability: a review of Australian experience and practice. Ecol. Eng., 36, 292–304. doi.10.1016/j.ecoleng.2009.04.006.

Hughes, S.A. (1993). Physical models and laboratory techniques in coastal engineering. World Scientific, London.

Hynes, H.B.N. (1970). The ecology of running waters. Toronto. University of Toronto Press. 555 pp.

Jowett, I. Richardson, J. (1990). Microhabitat preferences of benthic invertebrates in a New Zealand river and the development of in-stream flow-habitat models for Deleatidium spp. *New Zeal. J. Mar. Freshwat.*, 24: 19–30. doi.10.1080/00288330.1990.9516399.

Keylock, C.J., Constantinescu, G., Hardy, R.J. (2012). The application of computational fluid dynamics to natural river channels: Eddy resolving versus mean flow approaches. *Geomorphology*, 179, 1–20. doi.10.1016/j.geomorph.2012.09.006.

Kim, H.S., Kimura, I., Park, M. (2018). Numerical simulation of flow and suspended sediment deposition within and around a circular patch of vegetation on a rigid bed. *Water Resour. Res.*, 54, 7231–7251. doi.10.1029/2017WR021087.

Kitsikoudis, V., Kirca, V.S.O., Yagci, O., Celik, M.F. (2017). Clear-water scour and flow field alteration around an inclined pile. *Coast. Eng.*, 129, 59–73. doi.10.1016/j.coastaleng.2017.09.001.

Kitsikoudis, V., Yagci, O., Kirca, V.S.O. (2020). Experimental analysis of flow and turbulence in the wake of neighboring emergent vegetation patches with different densities. *Environ. Fluid Mech.*, 20, 1417–1439. doi.10.1007/s10652-020-09746-6.

Kitsikoudis, V., Yagci, O., Kirca, V.S.O., Kellecioglu D. (2016). Experimental investigation of channel flow through idealized isolated tree-like vegetation. *Environ. Fluid Mech.*, 16, 1283–1308. doi.10.1007/s10652-016-9487-7.

Knighton, A.D. (1972) Changes in a braided reach. *Bulletin of the Geological Society of America*, 83(12), 3813–3822. doi.10.1130/0016-7606(1972)83[3813:CIABR]2.0.CO;2.

Kollmann, J., Vieli, M., Edwards, P.J., Tockner, K., Ward, J.V. (1999). Interactions between vegetation development and island formation in the Alpine River Tagliamento. *Appl. Veg. Sci.*, 2, 25–36. doi.10.2307/1478878.

Larsen, B. E., Fuhrman, D. R., Sumer, B. M. (2016). Simulation of wave-plus-current scour beneath submarine pipelines. *J. Waterw. Port Coast. Ocean Eng.*, 142(5), 04016003.

Latrubesse, E.M., Stevaux, J.C. (2015). The Anavilhanas and Mariua archipelagos: fluvial wonders from the Negro River, Amazon Basin. In *Landscapes and Landforms of Brazil*, Vieira, B.C., Salgado, A.A.R., Santos, L.J.C., eds, Springer, p. 267p. doi.10.1007/978-94-017-8023-0_14.

Leigh, D.S. (2006). Terminal Pleistocene braided to meandering transition in rivers of the southeastern USA. *Catena*, 66(1–2), 155–160. doi.10.1016/j.catena.2005.11.008.

Leli, I.T., Stevaux, J.C. (2021). Lake-islands: a distinct morphology of river systems. *J. S. Am. Earth Sci.*, 111, 103424. doi.10.1016/j.jsames.2021.103424.

Leli, I.T., Stevaux, J.C., Assine, M.L. (2018). Genesis and sedimentary record of blind channel and islands of the Anabranching River: an evolution model. *Geomorphology*, 302, 35–45. doi.10.1016/j.geomorph.2017.05.001.

Leli, I.T., Stevaux, J.C., Assine, M.L. (2020). Origin, evolution, and sedimentary records of islands in large anabranching tropical rivers: the case of the Upper Parana River, Brazil. *Geomorphology*, 358, 107–118. doi.10.1016/j.geomorph.2020.107118.

Leopold, L.B Wolman, M.G. (1957). River channel patters: braided, meandering and straight. *U.S Geol. Surv. Prof. Pap.*, 282-B, pp. 39–85.

Li, Z., Wang, Z., Pan, B.; Zhu, H., Li, W. (2014). The development mechanism of gravel bars in rivers. *Quat. Int.*, 336, 73-79. doi.10.1016 /j.quaint.2013.12.039.

Liao, J.C. Cotel, A. (2013). Effects of Turbulence on Fish Swimming in Aquaculture. In *Swimming Physiology of Fish* Palstra, A., Planas, J., eds., Springer, Berlin, Heidelberg. doi.10.1007/978-3-642-31049-2_5.

Lloyd, N., Quinn, G., Thoms, M., Arthington, A., Gawne, B., Humphries, P., Walker, K. (2003) Does flow modification cause geomorphological and ecological response in rivers? A literature review from an Australian perspective. Technical Report 1 ⁄ 2004, CRC for *Freshw. Ecol.*, ISBN 0-9751642-02.

Lloyd, P.M., Stansby, P.K. (1997a). Shallow water flow around model conical islands of small side slope. I: Surface piercing. *J. Hydr. Eng.*, ASCE, 123(12), 1057–1067. doi.10.1061/(ASCE)0733-9429(1997)123:12(1057).

Lloyd, P.M., Stansby, P.K. (1997b). Shallow-water flow around model conical islands of small side slope. II: Submerged. *J. Hydraul. Eng.*, 123(12), 1068–1077. doi.10.1061/(ASCE)0733-9429(1997)123:12(1068).

Luchi, R., Zolezzi, G., Tubino, M. (2010). Modelling mid-channel bars in meandering channels. *Earth Surf. Process. Landf.*, 35, 902–917. doi.10.1002/esp.1947.

Lupandin, A.I. (2005). Effect of Flow Turbulence on Swimming Speed of Fish. *Biol. Bull. Russ. Acad. Sci.*, 32, 461–466. doi.10.1007/s10525-005-0125-z.

Maazouzi, C., Claret, C., Dole-Olivier, M.-J., Marmonier, P. (2013). Nutrient dynamics in river bed sediments: effects of hydrological disturbances using experimental flow manipulations. *J. Soils Sediments*, 13, 207–219. doi.10.1007/s11368-012-0622-x.

Majd, S.F., Yagci, O., Kirca, V.S.O., Kitsikoudis, V., and Lentsiou, E. (2016). Flow and turbulence around an inclined pile. In *Proceedings of the International Ocean and Polar Engineering Conference*; Rhodes, Greece.

McLaughlin, R.L. D.L.G. Noakes. (1998). Going against the flow: An examination of the propulsive movements made by young brook trout in streams. *Can. J. Fish. Aquat. Sci.*, 55: 853–860. doi.10.1139/f97-308.

Minshall, G.W. (1984) Aquatic insect-substratum relationships. In: Resh, V. H., Rosenberg, D.M. ed., The ecology of aquatic insects. New York. Praeger Publishers. 358–400.

Moir, K.J., Soulsby, C., Youngson, A.F. (2002). Hydraulic and sedimentary controls on the availability and use of Atlantic salmon (Salmo salar) spawning habitat in the River Dee system, north-east Scotland. *Geomorphology*, 45, 291–308. doi.10.1016/S0169-555X(01)00160-X.

Murray, A., Paola, C. (1994). A cellular model of braided rivers. *Nature*, 371, 54–57. doi.10.1038/371054a0.

Naiman, R.J., Decamps, H., Pollock, M. (1993). The role of riparian corridors in maintaining regional biodiversity. *Ecol. Appl.*, 3, 209-212. doi.10.2307/1941822.

Nakamura F. (2003). Restoration strategies for rivers, floodplains and wetland in Kushiro Mire and Shibetsu River, northern Japan. *Ecol. Civ. Eng.*, 5: 217–232 (in Japanese with English abstract). doi.10.3825/ece.5.217.

Nakano, D., Nakamura, F. (2008). The significance of meandering channel morphology on the diversity and abundance of macroinvertebrates in a lowland river in Japan. *Aquatic Conserv: Mar. Freshw. Ecosyst.*, 18, 780–798. doi.10.1002/aqc.885.

Nanson, G.C., Knighton, A.D. (1996). Anabranching rivers: their cause, character and classification. *Earth Surf. Process. Landf.*, 21, 217–239.

Nepf, H.M. (1999). Drag, turbulence, and diffusion in flow through emergent vegetation. *Water Resour. Res.*, 35(2), 479–489. doi.10.1029/1998WR900069.

Nicholas, A.P., Sambrook-Smith, G.H. (1999). Numerical simulation of three-dimensional flow hydraulics in a braided river. *Hydrol. Process.*, 13, 913–929.

Nie, H.W.De. (1987). The decrease in aquatic vegetation in Europe and its consequences for fish populations. EIFAC Occasional Paper 19. FAO, Rome, 88 pp.

Ock, G, Gaeuman, D, McSloy, J, Kondolf, G.M. (2015). Ecological functions of restored gravel bars, the Trinity River, California. *Ecol. Eng.*, 83, 49–60. doi.10.1016/j.ecoleng.2015.06.005.

Ouro, P., Wilson, C.A.M.E., Evans, P., Angeloudis, A. (2017). Large-eddy simulation of shallow turbulent wakes behind a conical island. *Phys. Fluids*, 29, 126601. doi.10.1063/1.5004028.

Poff, N.L., Zimmerman, J.K.H. (2010). Ecological responses to altered flow regimes: a literature review to inform the science and management of environmental flows. *Freshw. Biol.*, 55, 194–205. doi.10.1111/j.1365-2427.2009.02272.x.

Poff, N.L., Allan, J. D, Bain, M.B., Karr, J.R., Prestegaard, K.L, Richter, B., Sparks, R., Stromberg, J. (1997). The natural flow regime: a new paradigm for riverine conservation and restoration. *Bio. Sci.*, 47, 769–784. doi.10.2307/1313099.

Roulund, A., Sumer, B.M., Fredsøe, J., Michelsen, J. (2005). Numerical and experimental investigation of flow and scour around a circular pile. *J. Fluid Mech.*, 534, 351–401. doi.10.1017/S0022112005004507.

Ryan, D.K., Yearsley, J.M., Kelly-Quinn, M. (2013). Quantifying the effect of semi-natural riparian cover on stream temperatures: implications for salmonid habitat management. *Fish. Manage. Ecol.*, 20(6), 494–507. doi.10.1111/fme.12038.

Schoelynck, J., Groote, T.De., Bal K., Vandenbruwaene, W., Meire P., Temmerman, S. 2012. Self-organized patchiness and scale-dependent bio-geomorphic feedbacks in aquatic river vegetation. *Ecography*, 35, 760–768. doi.10.1111/j.1600-0587.2011.07177.x.

Skłodowski, M. Kiedrzyńska, E., Kiedrzyński, M., Urbaniak, M., Zielińska, K.M., Kurowski, J.K., Zalewski M. (2014). The role of riparian willows in phosphorus accumulation and PCB control for lotic water quality improvement. *Ecol. Eng.*, 70, 1-10. doi.10.1016/j.ecoleng.2014.03.088.

Smith, D.L., Goodwin, R.A., Nestler, J.M. (2014). Relating turbulence and fish habitat: A new approach

for management and research. *Rev. Fish. Sci. Aquac*., 22, 123–130. doi.10.1080/10641262.2013.803516.

Sumer, B.M., Fredsøe, J. (1997). Hydrodynamics Around Cylindrical Structures. World Scientific.

Surian, N., and Rinaldi, M. (2004). Channel adjustments in response to human alteration of sediment fluxes: examples from Italian rivers. In *Golosov*, Belyaev, V., Walling, D.E., eds., Sediment Transfer Through the Fluvial System, Publication 288. IAHS, 276–282.

Tal, M., Paola, C. (2007). Dynamic single-thread channels maintained by the interaction of flow and vegetation. *Geology*, 35 (4), 347–350. doi.10.1130/ G23260A.1.

Thornton, C.I., Abt, S.R., Clary, W.P. (1997). Vegetation influence on small stream siltation. *J. Am. Water Resour. Assoc.*, 33(6), 1279–1288. doi.10.1111/j.1752-1688.1997.tb03552.x.

Tooth, S., Nanson, G.C. (1999). Anabranching rivers on the Northern Plains of arid central Australia. *Geomorphology*, 29, 211–233. doi.10.1016/S0169-555X(99)00021-5.

Toth, L.A. (1993). The ecological basis of the Kissimmee River restoration plan. *Florida Scientist*, 56, 25–51.

Valyrakis, M., Liu, D., Turker, U., Yagci, O. (2021). The role of increasing riverbank vegetation density on flow dynamics across an asymmetrical channel. *Environ. Fluid Mech.*, 21, 643–666. doi.10.1007/s10652-021-09791-9.

Wilson, C.A.M.E, Yagci, O., Rauch, H.-P., Olsen, N.R.B. (2006). 3D numerical modelling of a willow vegetated river/floodplain system. *J. Hydrol.*, 327 (1–2), 13–21. doi.10.1016/j.jhydrol.2005.11.027.

Wintenberger, C.L., Rodrigues, S., Claude, N., Jugé, P., Bréhéret, J.-G., Villar, M. (2015). Dynamics of nonmigrating mid-channel bar and superimposed dunes in a sandy-gravelly river (Loire River, France). *Geomorphology*, 248, 185–204. doi.10.1016/j.geomorph.2015.07.032.

Wyrick, J.R., Klingeman, P.C., 2010. Proposed fluvial island classification scheme and its use for river restoration. *River Res. Applic*., 27, 814–825. doi.10.1002/rra.1395.

Yagci, O., Strom K. (2022). Reach-scale experiments on deposition process in vegetated channel: Suspended sediment capturing ability and backwater effect of instream plants. *J. Hydrol.*, 127612. doi.10.1016/j.jhydrol.2022.127612.

Yagci, O., Celik, M.F., Kitsikoudis, V., Kirca, V.S.O., Hodoglu, C., Valyrakis, M., Duran, Z., Kaya S. (2016). Scour patterns around isolated vegetation elements. *Adv. Water Resour.*, 97, 251-265. doi.10.1016/j.advwatres.2016.10.002.

Yagci, O., Yildirim, I., Celik, M.F., Kitsikoudis, V., Duran, Z., Kirca, V.S.O. (2017). Clear water scour around a finite array of cylinders. *Appl. Ocean Res.*, 68, 114–129. doi.10.1016/j.apor.2017.08.014.

Zhang, P., Qiao, Y., Grenouillet, G., Lek, S., Cai, L., Chang, J. (2021). Responses of spawning thermal suitability to climate change and hydropower operation for typical fishes below the Three Gorges Dam. *Ecol. Indic.*, 121, 107186. doi.10.1016/j.ecolind.2020.107186.